Università degli Studi di Padova

Dipartimento di Biologia

Corso di Laurea Magistrale in Biotecnologie Industriali

Characterization of a *Synechocystis sp. PCC 6803* strain expressing an algal Baeyer-Villiger monooxygenase

Relatore: Dott.ssa Elisabetta Bergantino

Dipartimento di Biologia

Correlatore: Dott. Mattia Niero

Dipartimento di Biologia

Controrelatore: Dott. Alessandro Alboresi

Dipartimento di Biologia

Laureanda: Eleonora Boccaletto

INDEX

4

1. Abstract - Riassunto

In this work, a *Synechocystis* sp. PCC 6803 strain, expressing the Baeyer-Villiger monooxygenase from *Cyanidioschyzon merolae*, (*Cm*BVMO) was characterized. The first step was the confirmation of *Cm*BVMO expression inside the cells, together with the evidence that the produced enzyme was catalytically active. This new strain, called Syn_zia_BVMO, exhibited an unexpected prolonged-growth phenotype when cultured in standard mixotrophic and autotrophic conditions. Some results, like the oxygen evolution rate and the PHB (polyhydroxybutirate) quantification, gave a hint about a possible increased NADPH-consumption activity of the cells. This capability would lead the strain to a higher photosynthetic efficiency and to an extra biomass production. Moreover, we identified a possible *in vivo* substrate for the activity of the heterologous enzyme: a *Synechocystis* strain expressing *Cm*BVMO and unable to synthetize hexadecanal, like the knockout mutant SynΔ*sll0209*, did not show a prolonged growth. It's possible that the *in vivo* substrate of *Cm*BVMO is hexadecanal, an intermediate of the alkane biosynthetic pathway. However, more evidences must be collected to support these hypothesis, f.i. using direct NADPH quantification methods and performing GC-MS analysis.

Nel presente lavoro è stato caratterizzato un ceppo di *Synechocystis* sp. PCC 6803 esprimente la Baeyer-Villiger monoossigenasi di *Cyanidioschyzon merolae* (*Cm*BVMO). Il primo passo è stata la conferma dell'espressione della proteina *Cm*BVMO nelle cellule e la prova che l'enzima prodotto è attivo cataliticamente. Questo nuovo ceppo, chiamato Syn_zia_BVMO, ha mostrato un inaspettato fenotipo di crescita prolungata quando messo in coltura in condizioni standard sia di mixotrofia che di autotrofia. Alcuni risultati, come la velocità di evoluzione di ossigeno e la quantificazione dei PHB (poliidrossibutirrati), hanno suggerito un possibile aumento nel consumo di NADPH nelle cellule. Questo aumenterebbe l'efficienza fotosintetica e la produzione di biomassa del ceppo. Inoltre, abbiamo identificato un possibile substrato per l'enzima *in vivo*: un ceppo di *Synechocystis* esprimente la proteina *Cm*BVMO e incapace di produrre esadecanale, come il mutante knock-out SynΔ*sll0209*, non ha mostrato la crescita prolungata. È possibile dunque che il substrato per *Cm*BVMO *in vivo* sia l'esadecanale, un intermedio della via di biosintesi degli alcani. Tuttavia, dovranno essere raccolte ulteriori prove a sostegno di queste ipotesi, per esempio usando metodi di quantificazione diretta del NADPH ed eseguendo analisi GC-MS.

2. Introduction

2.1 Cyanobacteria as tools for biotechnology

During the last decades cyanobacteria have been studied thoroughly by the scientific community, in particular as model organisms for deciphering the molecular basis of photosynthesis. These prokaryotes appeared roughly 3.5 billion years ago and were discovered to be the descendants of the first photosynthetic organisms on Earth. Their proliferation dramatically changed the composition of the atmosphere introducing molecular oxygen (the event is also known as the "oxygen catastrophe")(Flores, 2008). Moreover, according to the endosymbiotic theory, plastids originally derive from one of these cyanobacteria ancestors: around 1.5 billion years ago it was incorporated into a heterotrophic cell, giving birth to the first eukaryotic photosynthetic cell (Ochoa de Alda *et al.*, 2014).

Cyanobacteria are generally classified as Gram-negative bacteria, with a diameter ranging from 1 to 10 µm. The photosynthetic apparatus is located in the thylakoid membranes and comprises a unique type of light-harvesting complexes called phycobilisomes. They can be found in almost every terrestrial and aquatic environment, given their extreme diversification and ability to adapt to shifting conditions (Flores, 2008). The ongoing identification and genome sequencing of more and more cyanobacterial species made possible not only to shed light on the evolution and differentiation of these organisms, but also to allow genetic manipulation for basic and applied research. The increasing knowledge of the metabolic processes of these photosynthetic organisms and the development of tools for their genetic manipulation arose a potential biotechnological and industrial use of cyanobacteria.

Nowadays, the main organisms exploited in bioindustry are heterotrophic microorganisms like bacteria (e.g. *E. coli*) or yeasts (e.g. *S. cerevisae*), which require a carbon source of energy to synthetize the desired product. This feedstock often represents the main cost of the whole process, taking into account the pollution from their transport, their pre-treatment and, eventually, their limited commercial availability. The use of photosynthetic microorganisms would make the entire process environmentally and economically more sustainable. These organisms only need water, light and some micronutrients for growing, and sequestrate CO_2 from the atmosphere to synthetize the products of interest. The choice of cyanobacteria among other photosynthetic organisms is advantageous. Compared to terrestrial plants they are characterized by higher energy-to-biomass conversion efficiency, absence of non-photosynthetic (thus useless) tissues, no crop land competition and reduced use of water (Dismukes *et al.*, 2008). Compared to microalgae, they have a shorter life cycle, less articulated genomes, ease of transformation (Golden, Brusslan and Haselkorn, 1987) and possibility of exploiting existing secretion pathways for efficient product recovery.

The cyanobacterial species *Synechocystis* sp. PCC 6803 is one of the most studied, due to some advantages like ease of transformation and of integration of foreign DNA through homologous recombination. It can grow autotrophically (taking energy from light through photosynthesis), heterotrophically (consuming organic compounds in the medium, as source of energy) and even mixotrophically (both autotrophically and heterotrophically). Unlike other species, it doesn't perform nitrogen fixation (the conversion of atmospheric nitrogen to ammonia and nitrates) and it's ubiquitously present in freshwater reservoirs, with an optimum growth temperature of 30° C and pH range of 7-8. The complete sequence of its genome became available in 1996 (Kaneko *et al.*, 1996), which placed it in the fourth position among the genomes completely sequenced and the first among phototrophic organisms. It comprises a circular 3.5-million-bp-long chromosome and seven plasmids, and was recognized to be polyploid, having an estimated number of genome copies up to 200 (Griese, Lange and Soppa, 2011). The information of gene structure and gene function has been deposited in two genome databases, CyanoBase and CyanoMutants respectively (Ikeuchi and Tabata, 2001).

2.1.1 Production of biofuels and high-value compounds

The unsustainability concerns of fossil fuels pose a great challenge about where to find adequate energy-dense substitutes. The production of biofuels in cyanobacteria could be part of the solution, since it would be CO_2-neutral and potentially up-scalable to very large volumes. One of the first attempts focused on bioethanol production and the optimization of the process is currently proceeding (Luan *et al.*, 2015). Bioethanol is the main biofuel today in terms of quantity, and there's an impelling need to overcome all the issues connected with its production from plant feedstocks (Deng and Coleman, 1999). Other alcohols like isobutanol (Li, Shen and Liao, 2014) and fatty alcohols (Yao *et al.*, 2014) were also synthetized with a high yield. Alkanes, the main components of fossil-derived fuels, were obtained from cyanobacteria more recently (Yoshino *et al.*, 2014). The most investigated pathway for its potential in biodiesel production is the one leading to free fatty acids (Liu, Sheng and Curtiss III, 2011; Ruffing, 2014; Work *et al.*, 2015).

During the last years, also hydrogen gained attention as biofuel, for its high energy density. Cyanobacteria naturally possess H_2-evolving NAD(P)H-consuming enzymes, called hydrogenases, that can be exploited in two main ways: performing photofermentation of organic acids (Stephen *et al.*, 2017) or using NADPH from the electron transport chain in autotrophic growth (Ainas *et al.*, 2017). In N_2-fixing cyanobacteria there's another class of exploitable H_2-evolving enzymes: nitrogenases. Even though a considerable light-to-H_2 efficiency was achieved in some strains by deleting H_2-consuming enzymes (Kosourov, Murukesan and Allahverdiyeva, 2017), the high energy required for N_2 fixation makes this process not sufficiently improvable.

Since petroleum is the source of many bulk and fine chemicals that are essential for various industrial sectors, there's the need to find a bio-based substitute for them too. Some are naturally produced by cyanobacteria, thus the main aim of the engineering is boosting the specific pathway to get the highest productivity. Other chemicals require the genetic introduction of one or more proteins (and in some cases even entire pathways). Many efforts focused on the biopolymers synthesis, in particular of polyhydroxyalkanoates (PHAs) since many cyanobacteria naturally produce them. Up to now the cyanobacterial pathways for the synthesis of PHAs have been studied and modified for the production of: the monomer 3-hydroxypropionic acid (Wang *et al.*, 2016); the polymer polyhydroxybutirate (PHB) with an impressive 85% accumulation on dcw (dry cell weight) (Samantaray and Mallick, 2012) ; the co-polymer poly(3-hydroxybutirate-co-3-hydroxyvalerate) with 77% accumulation on dcw (Bhati and Mallick, 2015). These yields however were reached adding organic carbon substrates like acetate, while in photoautotrophic conditions PHA accumulation has been optimized at 12% so far (Carpine *et al.*, 2017). Other fossil-based chemicals for which a biosynthetic pathway has been found in cyanobacteria are terpenoids, used as industrial additives and fuel components. Pathway engineering and carbon flux optimizations were performed, aiming to obtain significative amounts of limonene and bisabolene (Davies *et al.*, 2014), squalene (Choi *et al.*, 2016), beta-phellandrene (Formighieri and Melis, 2016) and especially isoprene, the main component of rubber (Bentley, Zurbriggen and Melis, 2014; Pade *et al.*, 2016; Chaves *et al.*, 2017).

The main hurdle to the industrial scaling up of all the aforesaid processes is the economic feasibility. The productivity, despite the great advances, is still low and thus it's not competitive with the fossil-based industry. The co-production of high value compounds is a possible mean by which rising the ROI (return of investment). Examples of high-value compounds whose production in cyanobacteria could be advantageous are: antioxidant nutraceuticals like carotenoids (Wang, Kim and Kim, 2014); antimicrobials of various chemical classes like alkaloids, cyclic or aromatics compounds (Swain, Paidesetty and Padhy, 2017); antivirals like lectins (R. S. Singh *et al.*, 2017); antitumorals, like simple peptides or complex macrocyclic polyethers (Simmons *et al.*, 2005); anti-inflammatories like some fatty acid derivatives (Manivannan, Muralitharan and Balaji, 2017).

Eventually, the use of high-throughput analysis and systems biology approaches, such as transcriptomics, proteomics and metabolomics, will give an important impulse to the improvement of productivity and photosynthetic efficiency.

2.1.2 Expression of heterologous proteins and biocatalysis

Cyanobacteria are emerging also as photosynthetic factories to produce proteins, a green alternative to traditional bacterial hosts. Moreover, given the extensive thylakoid membrane system of cyanobacteria, they are good candidates for the expression of membrane proteins. This class of proteins is the hardest to produce in sufficient quantity for crystallization and thus structural characterization. The main issue for this application is the lack of knowledge of sufficiently strong promoters, both native and artificial (Angermayr and Hellingwerf, 2013), but new bioinformatic and whole-genome analysis are helping in the search of native efficient promoters. For instance, Zhou and his group recently discovered a super-strong promoter which led to the 15% of production of the desired protein in total soluble fraction: this result is comparable to *E. coli* production levels (Zhou *et al.*, 2015).

The production in good yield of heterologous enzymes offers to cyanobacteria new potential applications in biocatalysis.

Biocatalysis is the process in which natural catalysts, such as enzymes, are used to perform chemical transformations on organic compounds. It's a greener (and thus preferred) alternative to conventional chemical synthesis, considering some important advantages like: milder reaction conditions (room temperature and physiological pH), use of water as solvent, reduced production of waste, renewable and less toxic feedstocks and reduced number of operational steps (Sheldon and Woodley, 2017). Moreover, the chiral nature of enzymes results in high chemo-, regio- and stereo-selectivity, providing only the desired enantiomer and not racemic mixtures that require further processing.

To assess the actual efficiency of the enzymatic reaction, several parameters must be taken into account: specific activity (quantified by the catalytic constant k_{cat} = max rate of product formation), specificity (k_{cat} /K_M = efficiency of conversion for the given substrate), stability and degree of substrate and/or product inhibition (Koeller and Wong, 2001). The ideal biocatalyst would be highly active and specific towards the substrate, with a high stability and minimal substrate/product inhibition.

In order to perform a biocatalytic process, there are three main strategies regarding the format of the biocatalyst: isolated enzymes, immobilized enzymes and resting whole cells (Fig. 1 a,b,c respectively). In the first one the enzyme is used outside of the cell in which it was produced, thus it must be secreted or separated from the debris after cell disruption (Fig. 1 a). In cyanobacteria, this method has been applied recently: an esterase and a carboxylase were successfully produced in *Synechocystis* sp. PCC 6803 and proved to be fully enantioselective (Bartsch *et al.*, 2015). Nevertheless, optimization of the extraction methods has to be further improved to retrieve higher amounts of total initial proteins (Field *et al.*, 2017).

(a) Isolated enzyme biocatalysis

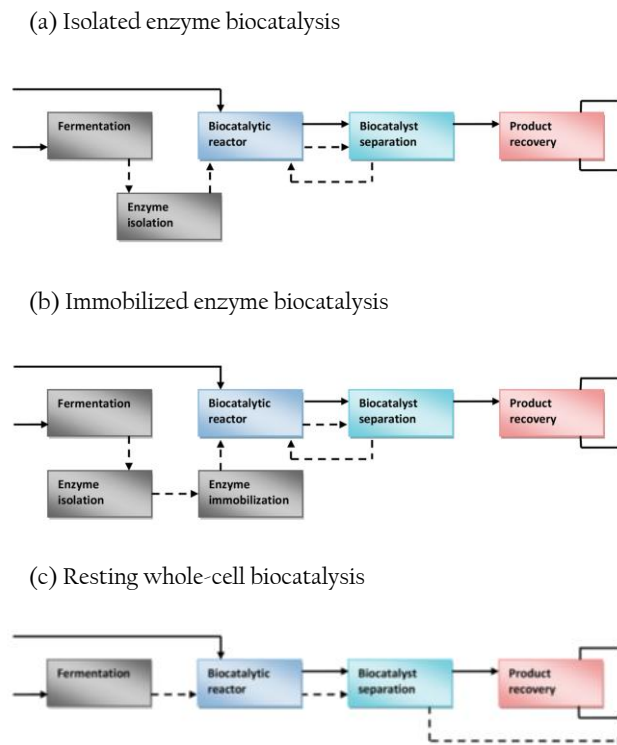(b) Immobilized enzyme biocatalysis

(c) Resting whole-cell biocatalysis

Figure 1: Flowsheets of the three classes of biocatalysis. Solid lines indicate substrate-/product-rich streams. Dotted lines indicate biocatalyst streams.
(Image from Sheldon and Woodley, 2017)

In many cases, the cost of the enzyme is such that reuse is necessary, and this can most effectively be achieved using an immobilized enzyme (Fig. 1 b). The immobilization of the enzyme, on a spherical solid or within a porous support, facilitates its removal from the product stream by simple filtration, and enable subsequent recycle (performed in some cases more than 100 times). However, in both these modes of operation there's a significative issue about the cofactors, indispensable for most reactions: for instance, oxidoreductions necessitate reducing equivalents (NADH, NADPH) in sufficient quantity, at least equimolar to the substrate. The straightforward answer is cofactor regeneration. In most of the cases the desired reaction is coupled with a second enzyme that restores the cofactor, consuming a given "sacrificial" substrate. Other new intriguing alternatives are emerging, like photo-catalytic regeneration (X. Wang *et al.*, 2017) and cofactor engineering (M. Wang *et al.*, 2017).

Considering all the steps, variables and parameters, process optimization for isolated- and immobilized-enzyme biocatalysis is usually very complex and time-consuming, and thus the third strategy comes as an alternative. In resting cells biocatalysis the reaction is performed in whole-cell format, following cell growth (Fig. 1 c). Fundamental advantages are: reduced number of operational steps, no need for extraction or enzyme purification, avoidance of the inactivity issues of enzyme immobilization, no added cofactor regeneration systems (supplied by the cell itself) and thus no sacrificial substrate. Generally, the consequences are: higher

enzyme stability, lower costs, faster lab-to-industry scaling, lower energy demand, higher atom efficiency, easier downstream processing. Whole-cell biocatalysis is the most suitable option for some applications, f.i. enzymatic reactions that require expensive cofactors like NADPH. Moreover, it can be efficiently exploited for multistep conversions, by exploiting existing pathways of the host or by introducing novel ones (Lin and Tao, 2017), and for the production of many compounds from a single microorganism (Bode *et al.*, 2002). Besides, the use of solvent-tolerant hosts may provide an efficient solution to the conversion of lipophilic compounds (de Carvalho, 2017). However, whole-cell biocatalysis may manifest some serious problems: competition with endogenous enzymes for the use of the substrate and/or the cofactors, undesired product modifications, diffusional limitations through cell membrane. Nevertheless, the extensive work done with *E. coli* shows great results, even in scalability and sequestration of substrate/product to prevent enzyme inhibition (Baldwin, Wohlgemuth and Woodley, 2008; Geitner *et al.*, 2010). On the other hand, cyanobacteria, as a greener version, have attracted more and more attention, e.g.: for the asymmetric reduction of ketones (Nakamura *et al.*, 2000; Havel and Weuster-Botz, 2006), for various bioconversions of monoterpenes (Balcerzak *et al.*, 2014) and for the enantioselective reduction of phosphonates (Górak and Żymańczyk-Duda, 2015). As a further important advantage, cyanobacteria have a rich pool of NADPH, thus they are the perfect candidates for NADPH-dependent biocatalysts. It's the case of a vast class of incredibly useful enzymes: monooxygenases. A recent work (Böhmer *et al.*, 2017) has shown the feasibility of biotransformation with the cyclohexanone monooxygenase from *Acinetobacter calcoaceticus* (CHMO) in *Synechocystis* sp. PCC 6803, with specific activity values almost equal to those obtained in *E. coli* and no negative effects on cells viability. This work also pointed out some issues that need to be overcome, like undesired side reactions and cell-density limitation. To exploit the uniquely abundant NADPH pool of cyanobacteria, another possibility is changing the cofactor specificity of the enzyme from NADH to NADPH (Park and Choi, 2017).

2.2 Baeyer-Villiger monooxygenases

As mentioned, monooxygenases are a fascinating vast class of enzymes; they are able to catalyse the transfer of one atom of oxygen to an organic substrate, and reduce the other atom of oxygen to water. They are promising biocatalysts for the synthesis of organic molecule since this kind of insertion is hard to achieve in a chemical way (in some cases even unfeasible). Among the specific reactions catalysed by these enzymes, we can find the Baeyer-Villiger oxidation, in which ketones or aldehydes are oxidized into the corresponding esters or lactones, resulting in oxygen insertion next to the carbonyl group. Baeyer-Villiger monooxygenases (BVMOs) need a flavin cofactor (FAD/FMN) and a source of reducing potential (NADPH/NADH), and depending on these cofactors usage they
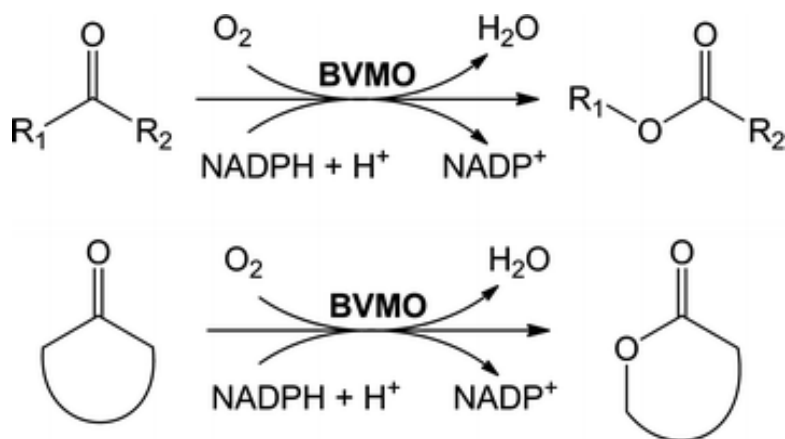
Figure 2: Mechanism of action of Type I BVMOs on a linear ketone (upper reaction) and on a cyclic ketone (lower reaction). Image from Ceccoli et al. 2017

are classified in Type I (FAD and NADPH dependant) and Type II (FMN and NADH dependent)(Willetts, 1997).

Type I BVMOs have been more studied because of their high regio-, chemo- and stereo-selectivity (Bučko *et al.*, 2016), together with broad substrate scope, meaning that a single enzyme can act on multiple diverse substrates (Fig. 2). These enzymes contain two dinucleotide-binding domains (βαβ-folds) known as Rossmann motifs, one for the FAD binding and the other for the NADPH binding (Fraaije *et al.*, 2002). More than 50 protein sequences of this class are available for recombinant expression today. The cyclohexanone monooxygenase (CHMO) from *Acinetobacter* species (Donoghue, Norris and Trudgill, 1976) is one of the first BVMOs that has been discovered and hence it's one of the most studied. CHMO homologs have been found in many prokaryotes from almost every phyla (Kyte *et al.*, 2004). Other BVMOs were then identified and thoroughly characterized, like the steroid-MO (monooxygenase) from *Rhodococcus* (Morii *et al.*, 1999) and the 4-hydroxy-acetophenone-MO from *Pseudomonas fluorescens* ACB (Kamerbeek *et al.*, 2001). The phenylacetone-MO (PAMO) from the thermophilic bacterium *Thermobifida fusca* was the first Type I BVMO whose crystal structure has been determined (Malito *et al.*, 2004), while one of the last BVMOs discovered and structurally resolved is the polycyclic-ketone-MO from the thermophilic fungus *Thermothelomyces thermophila* (Fürst *et al.*, 2017).

2.2.1 New Type I BVMOs: *Cm*BVMO and *Pp*BVMO

As the protein sequences started to accumulate, bioinformatic approaches became more and more trustworthy for the identification of new BVMOs. Multiple sequence alignment analysis showed that Type I BVMOs can be identified using a specific sequence motif: FxGxxxHxxxWP (Fraaije *et al.*, 2002). Many of the aforementioned BVMOs were discovered through whole-genome search of this

motif, together with a good sequence similarity to known BVMOs (this method is called "genome mining").

In the laboratory where I did my internship, two new BVMOs were identified using this method, then cloned and characterized (Beneventi *et al.*, 2013). One of this enzyme was obtained from the red alga *Cyanidioschyzon merolae* (*Cm*) and the other one from the moss *Physcomitrella patens* (*Pp*). Photosynthetic eukaryotes are very uncommon sources for BVMOs. In fact, only two BVMOs from eukaryotic origin had been cloned and expressed by the date of the Beneventi *et al.* work: the cycloalkanone monooxygenase from *Cylindrocarpon radicicola* ATCC 11011 (Leipold, Wardenga and Bornscheuer, 2012) and the BVMO from *Aspergillus fumigatus* Af293 (Mascotti *et al.*, 2013). Other eukaryotic BVMOs were investigated since then, but actually almost all of them have been found in fungi (Romero *et al.*, 2016; Bordewick *et al.*, 2017). A wide screening of fungal species revealed that 80% are positive for the presence of BVMO genes (Butinar *et al.*, 2015). These fungal enzymes are likely to take part in several biodegradation processes, activity in which fungi are key players. Nevertheless, the discovery of BVMOs in photosynthetic eukaryotes remains unique up to now and poses new questions about the physiological function of these enzymes.

The biochemical characterization of *Cm*BVMO is particularly relevant for the purposes of this thesis. This enzyme has a melting temperature (Tm) of 56° C, which is considerably higher than that of most known BVMOs. Considering that *Cyanidioschizon merolae* is a red alga living at 45-56 °C (Ciniglia *et al.*, 2004), this result was not unexpected. Moreover, a recent work showed that also phycocyanins from *C. merolae* have almost the same Tm (Rahman *et al.*, 2017). The biocatalytic characterization of *Cm*BVMO, including substrate profiling, steady-state kinetics and conversions, showed the preference of this enzyme for linear aliphatic ketones (C8 and C12) (Fig. 3). Conversion of these ketones resulted in the formation of the expected ester product, fully obeying the stereochemical rule of Baeyer-Villiger reactions, according to which the migrating group is the most substituted (Fig. 4). Looking at the catalytic performance, the considerable low values of the kinetic parameters (K_M, k_{cat}, k_{cat}/K_M) suggested a potential role of the enzyme in the secondary metabolism. Indeed, it is generally assumed that the selective pressure acting on non-central metabolism pathways is sensibly weaker than the one acting on essential ones, so allowing "secondary" enzymes to retain low or moderate rates of reaction. The actual role of *Cm*BVMO in the red alga is not known but, as mentioned above for fungal BVMOs, it is likely involved in catabolic reactions. The substrate preferences of the enzyme point toward linear alkanones, which are structurally similar to side chains of chlorophylls and pheophytins. Hence, it can probably be involved in modifications of photosynthetic pigments *in vivo*. However, deeper studies are needed to clarify its physiological function, f.i. by engineering and analysing knock-out mutants of *C. merolae.*

Substrate		K_M [mM]	k_{cat} [s^{-1}]	k_{cat}/K_M [s^{-1} mM]
2-Dodecanone		0.004 ± 0.001	0.383 ± 0.018	90.8
Octanal		0.010 ± 0.008	0.252 ± 0.043	25.3
2-Octanone		0.011 ± 0.006	0.250 ± 0.031	22.7
3-Octanone		0.0030 ± 0.0005	0.210 ± 0.006	70
4-Octanone		0.0040 ± 0.0009	0.202 ± 0.006	50.5
4-(4-Hydroxyphenyl)-2-butanone		0.0070 ± 0.0007	0.079 ± 0.002	11.2
Bicyclo[3.2.0]hept-2-en-6-one		0.0040 ± 0.0007	0.085 ± 0.002	21.3
3-Phenylpentane-2,4-dione		0.099 ± 0.026	0.015 ± 0.001	0.2
Phenylacetone		0.097 ± 0.071	0.032 ± 0.006	0.3

Figure 3: Steady-state kinetic analysis of CmBVMO on various substrates. From Beneventi et al. 2013

Substrate	Product	Conversion (%)
		Cm
		–
		80
		100
		100
		100
		100

Figure 4: Conversion of CmBVMO on some identified substrates and corresponding products. From Beneventi et al. 2013

2.3 Construction of the Syn_zia_BVMO strain

To further study this newly discovered monooxygenase and to explore its possible biocatalytic applications, the gene sequence of *Cm*BVMO was cloned in *Synechocystis* sp. PCC 6803. As previously mentioned, cyanobacteria are ideal for harbouring NADPH-consuming enzymes, and thus this species appeared as a reasonable choice. *Synechocystis* sp. PCC 6803 is well-characterized, easy to be genetically manipulated and characterized by a flexible metabolism: when supplied with glucose it grows exponentially faster than in the absence of glucose.

Thus, an expression plasmid was designed, aiming to introduce through homologous recombination the desired gene (*Cm*BVMO) together with a selection marker (Kan^R, the gene for Kanamycin resistance) into the genome of *Synechocystis* sp. PCC 6803 (hereafter *Synechocystis*).

The genomic region downstream the NADH dehydrogenase gene (*ndhB*, gene *ssl0223*) was chosen as site for the recombination. This region is considered a neutral site, since is interrupted by other foreign sequences was already demonstrated to not generate unexpected phenotype, keeping genetic and transcriptomic perturbations at the minimum (Aoki, Kondo and Ishiura, 1995; Kucho *et al.*, 2005; Tsujimoto, Kamiya and Fujita, 2016). However, it must be said that inserting DNA constructs here causes the knock-out of an open reading frame coding an unknown putative protein of 90 aminoacids (*ssl0410*, according to CyanoBase database).

In order to explore the chance to induce the expression of *Cm*BVMO gene, the *zia*A operator-promoter was chosen for the recombinant gene. In *Synechocystis* some metal-responding promoters have been investigated (Blasi *et al.*, 2012), among which the zinc-responding *zia*A operator-promoter has been described with a low basal expression level. In absence of Zn^{2+} ions, its repressor ZiaR binds to the operator sequence blocking the transcription, while in presence of Zn^{2+} ions ZiaR detaches and transcription starts (Busenlehner, Pennella and Giedroc, 2003).

The final transformation vector for the integration of the recombinant gene *zia*P/O-*Cm*BVMO into *Synechocystis* genome was called pDEV_zia_BVMO (were pDEV stands for Direct Expression Vector). Summarizing, it is composed by two portions of the chosen neutral region (NR1 and NR2), the inducible promoter *zia*A, the coding sequence for the enzyme *Cm*BVMO and the kanamycin resistance cassette (Kan^R).

The sequence engineered for recombination was excised from the rest of the plasmid to improve the recombination efficiency, and then used to transform a wild-type strain of *Synechocystis*. The selection of the recombinant colonies was performed in Petri dishes containing 10 μg/ml kanamycin. Single colonies from the initial transformation were re-streaked ten times on increasing concentrations of

antibiotic (up to 50 µg/ml). This subcloning operation is necessary to achieve homoplasmy, given the high copy number of *Synechocystis'* genome.

At the end of the selection process, homoplasmy was checked by PCR, confirming the total absence of wild-type copies of the genome in the recombinant colonies.

This new strain was thus called Syn_zia_BVMO (Fig. 5).

Figure 5: Schematic representation of the neutral site after the recombination, in the resulting new strain Syn_zia_BVMO.

3. Aim of the thesis

This work is focused on the thorough characterization of the cyanobacterial Syn_zia_BVMO strain. First, expression of *Cm*BVMO and inducibility of the *ziaA* promoter were investigated by Western Blot and mRNA analysis. The growth profile of this new strain was then analysed in mixotrophic and autotrophic liquid cultures. The results showed an unexpected enhanced growth of Syn_zia_BVMO compared to the wild type, and these results were also confirmed by dry cell weight measures. This increased biomass-accumulating strain became then attractive for biocatalytic purposes, since a possible increase in productivity could be realised. Therefore, elucidating the causes of this behaviour could be extremely useful. First of all, it could help achieving a deeper understanding of molecular processes inside this cyanobacterium. Then, these findings could provide precise indications for further biotechnological engineering, especially for biocatalytic aims.

The characterization went through a morphological macroscopic observation with TEM (Transmission Electron Microscopy), and then the drawing of a growth curve under a different light condition. With the use of an enzymatic activity assay and a native-polyacrylamide-gel electrophoresis (native-PAGE), the effective activity of *Cm*BVMO inside the strain was verified. This was done in order to support possible links between the heterologous enzyme and the prolonged-growth phenotype.

A possible explanation for the unpredicted behaviour of the recombinant strain was evaluated, pointing towards a correlation with NADPH content. To verify this, measures of oxygen evolution were performed. Moreover, the content in reducing equivalents was estimated exploiting polyhydroxybutirate (PHB) synthesis, which occurs in *Synechocystis* when limited-growth conditions are applied.

To justify an *in vivo* activity of *Cm*BVMO, a suitable substrate was searched inside *Synechocystis* cells, and indeed a compatible compound was noticed. To elucidate its possible involvement, mutant strains were created, targeting an enzyme of the biosynthetic pathway of this substrate. Knockout constructs with resistance cassettes were assembled and then introduced through homologous recombination. Homoplasmy was verified via PCR after the last selection passage. Growth of these mutants was then monitored in liquid cultures and measures of PHB content were also performed.

4. Results

4.1 General characterization

The first part of the work focused on characterizing the new Syn_zia_BVMO strain, the *Synechocystis* strain expressing the BVMO from *Cyanidioschyzon merolae*. A preliminary investigation on the activity of the recombinant enzyme *Cm*BVMO inside the cyanobacterial cells was also performed.

4.1.1 Expression of *Cm*BVMO: RT-PCR and Western blot analysis

The study started verifying the actual presence of the enzyme, firstly in the form of transcript mRNA (RT-PCR) and then as protein (Western blot). Moreover, given the presence of the *ziaA* promoter upstream the *Cm*BVMO ORF (see par. 2.3), the promoter inducibility by Zn^{2+} ions had to be checked.

For the mRNA analysis, liquid cultures of each strain (wt and Syn_zia_BVMO) were subjected to three different Zn^{2+} concentrations: (1) 0 µM, in a modified BG11 medium without zinc; (2) 1,3 µM, in normal BG11 medium; (3) 5,3 µM, in a modified BG11 medium with added 4 µM of zinc. BG11 medium is commonly used for *Synechocystis* (Rippka *et al.*, 1979). After 24 hours of growth, samples from each condition and strain were processed to purify total RNA. Then, the RNA pool was retro-transcribed with random primers and the resulting cDNA was used as template for the amplification by PCR, in two separate reaction using BVMO-specific or the PetB-specific primers. The first reaction was needed to check the presence of the BVMO transcript while the second one was used to normalize the intensity of the BVMO band in relation to a housekeeping gene (PetB: cytochrome b_6). The agarose gel electrophoresis of the PCR products is presented in Figure 11.

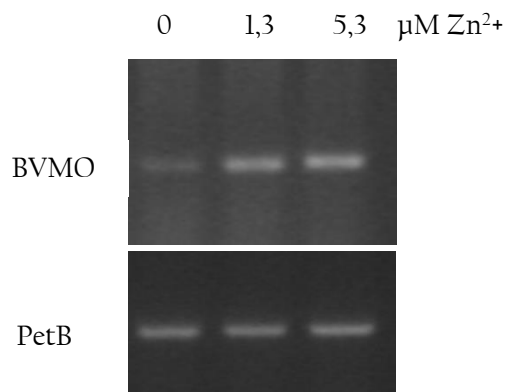*Figure 11: Agarose gel electrophoresis of PCR products obtained by using BVMO- and PetB-specific primers on cDNA from Syn_zia_BVMO. Concentrations of zinc ions in the respective culture medium are reported above.*

The first observation is that the transcript for CmBVMO is present in the recombinant strain in normal BG11 medium (1,3 µM), which is the condition in which *Synechocystis* cells are normally kept. Secondly, the presence of the transcript in cells grown in the absence of zinc ions shows that the *ziaA* promoter is partially leaky. Finally, the intensity of the band from the culture with added zinc appears almost equal to the one from normal BG11 culture.

Given the presence of the CmBVMO transcript, a Western blot was used to check the presence of the translated protein. The liquid culture conditions of both strains were exactly as those used for the RNA extraction, in particular for Zn^{2+} concentrations (1) and (3) (0 and 5.3 µM). After 48 hours of growth, samples from every culture were treated to obtain a total protein extract, which was then quantified via Bradford colorimetric assay. Based on this quantification, 75 µg of total proteins were loaded in each lane of a SDS-PAGE gel. After the electrophoretic run and the blotting procedure, incubation of the membrane with a BVMO-specific polyclonal antibody allowed ultimately the visualization of the bands (Fig. 12). The result showed the presence of the protein in the recombinant different intensities. Thus, the expression of CmBVMO and the leakiness of the *ziaA* promoter were both confirmed.
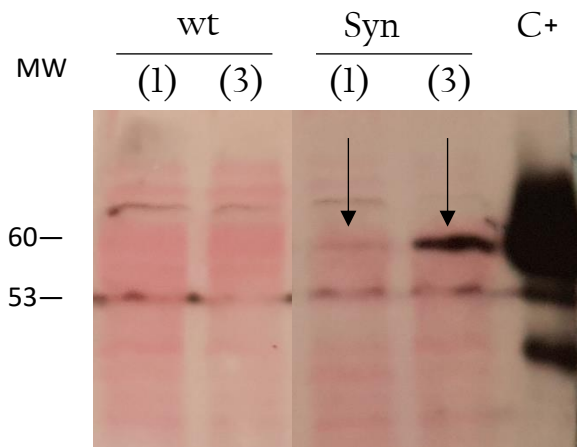

Figure 12: Western Blot of wt and Syn_zia_BVMO, developed by using BVMO-specific polyclonal antibody. The positive control (C+) in the last lane is given by purified CmBVMO expressed in E. coli. MW: indication of the molecular weight

4.1.2 Growth curves and dry cell weight

It was necessary to check for possible harmful effects of CmBVMO on *Synechocystis* cells, since it's an exogenous protein. Hence, the growth profile of the recombinant strain was drawn. BG11 liquid medium was supplemented with glucose to establish mixotrophic conditions. The concentration of cells was then monitored measuring the optical density (OD), as generally done with bacterial cells. Cultures were

incubated in constant agitation at 30°C, with a light intensity of 30 µE s^{-1}m^{-2}. This growth conditions will be hereafter called "standard" conditions.

The results are presented in Fig. 7, where the graph shows that the recombinant strain presented a longer growth phase compared to the wild-type (wt). The difference in optical density (OD) started at day 6-7 and became more relevant from day 10-11 on. At the early stationary phase of the recombinant strain, the OD was almost double compared to the wt.
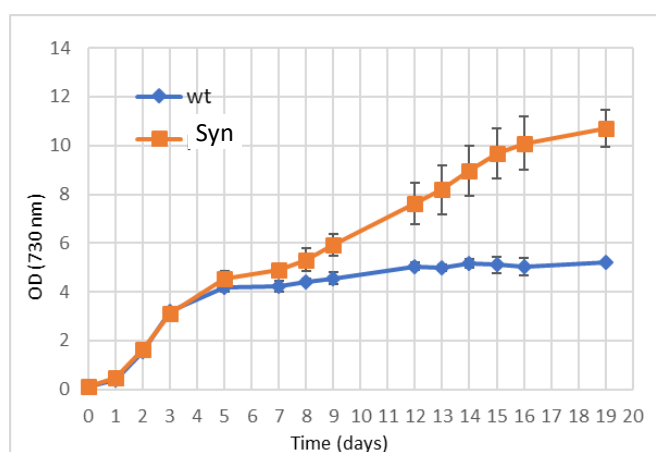

Figure 7: Growth curves of the wild-type (wt) strain and of the Syn_zia_BVMO strain in BG11 medium with 5mM glucose, measured by registering the absorbance at 730 nm. The values reported are means of three independent experiments, with relative standard error bars.

To assess whether or not this behaviour was present only under mixotrophy, a growth experiment in autotrophic (phototrophic) conditions was performed. In this case, the growth conditions differed from the mixotrophic ones for the absence of glucose in the BG11 medium. The obtained growth curves had the same trend of those registered in mixotrophy, with the recombinant strain reaching higher cell densities at the stationary phase (Fig. 8).
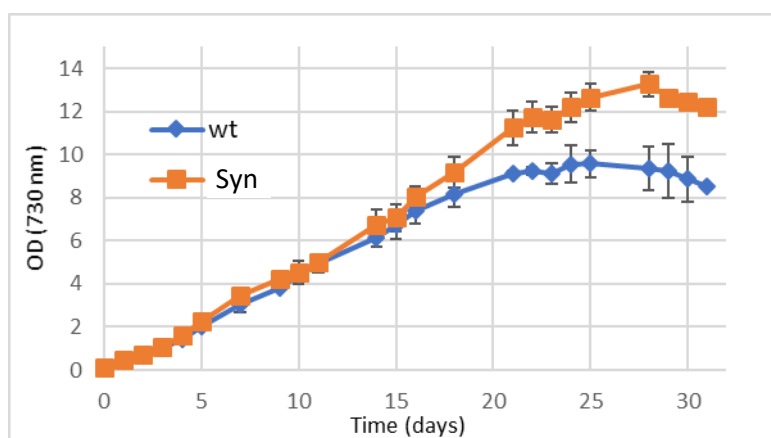

Figure 8: Growth curves of the wild-type (wt) strain and of the Syn_zia_BVMO strain in BG11 medium in abscence of glucose, measured by registering the absorbance at 730 nm. The values reported are means of three independent experiments, with relative standard error bars.

To verify whether the measured optical densities corresponded to biomass production, total biomass was quantified as dry cell weight (DCW) per volume of liquid culture. The DCW of both the strains, was measured at day 4, 11 and 15 of the mixotrophic growth. These three time-points were chosen as representative of the early, middle and late stationary phase of the wild type strain. The Syn_zia_BVMO strain showed an increase in mg(dcw)/ml, in accordance to the growth profiles (Fig. 9). The obtained values confirmed that the observed increase in OD is due to an increased biomass production. At day 11 and 15, an extra biomass formation of approximately 0.6 g/l and 1,4 g/l was registered, respectively.
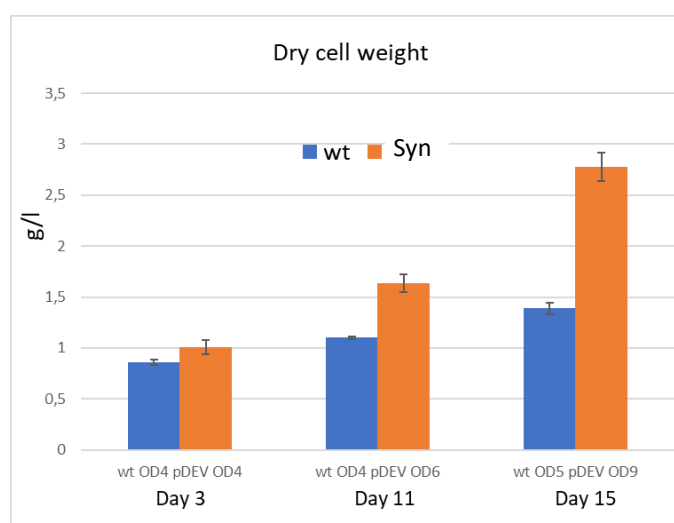

Figure 9: Dry cell weight of mixotrophic culture of wt and Syn_zia_BVMO. The OD value of each strain is reported for every day of sampling. The values reported are means of three independent experiments, with relative standard error bars.

4.1.3 Growth curves under high light intensity

In the characterization of photosynthetic organisms, light intensity plays a pivotal role. Growth curves under different light conditions may vary significantly. To check the behaviour of the Syn_zia_BVMO strain under such conditions, growth curves were set in mixotrophic and also phototrophic conditions, under an illumination of 200 $\mu E\ m^{-2}\ s^{-1}$. This saturating intensity will be termed as "high light". The other parameters remained those of the standard setting. The graphs show that the growth profiles of the wt and the recombinant strain are almost identical, both in mixotrophy and in autotrophy (Fig. 17). Therefore, Syn_zia_BVMO strain did not manifest any peculiar phenotype in high light conditions.
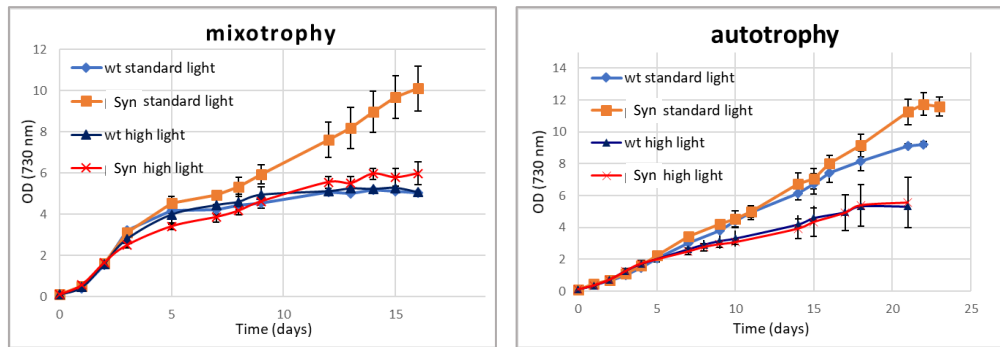
Figure 17: Growth curves of the wt and Syn_zia_BVMO strain at a light intensity of 200 μE m^{-2} s^{-1}, measured by registering the absorbance at 730 nm. The values reported are means of three independent experiments, with relative standard error bars.

4.1.4 Electronic Microscopy images

Given the macroscopic difference in the standard growth curves, a legit question arose about possible morphological changes (f.i. about number and shape of the thylakoid membranes) between the two strains, the wt and the recombinant one. Hence, using the TEM (Transmission Electron Microscopy) technique, images of the two strains were collected. Samples were taken from mixotrophic cultures at day 4 and at day 11, as previously done for the dry cell weight measures. Some of the images are presented (Fig. 10). The TEM analysis doesn't show any significative differences: the Syn_zia_BVMO strain doesn't exhibit visible morphological alterations compared to the wild type strain.
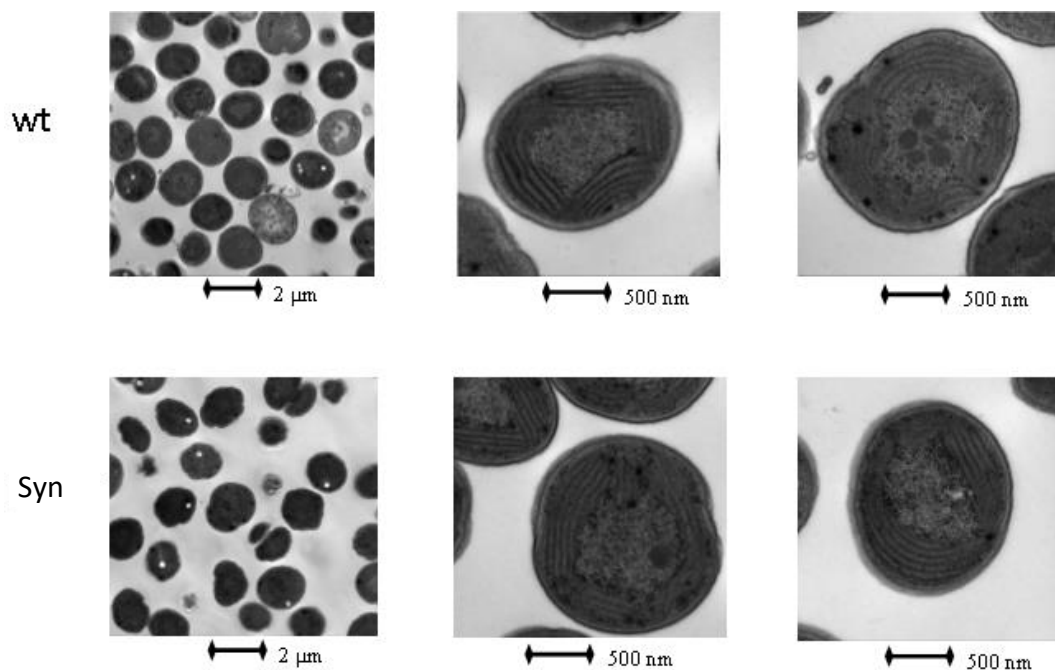

Figure 10: TEM microscopy images of wt and Syn_zia_BVMO cells.

4.1.5 *Cm*BVMO activity in *Synechocystis*

In order to link the observed phenotype to *Cm*BVMO, it was needed to assess if the enzyme was correctly folded and catalytically active in *Synechocystis.* Thus, the protein was purified and subjected to a direct activity assay. Moreover, a native gel electrophoresis was carried out, followed by a colorimetric activity assay. For both the assays, 3-nonanone was chosen as substrate, due to the high activity previously reported in the *in vitro* assay (Beneventi *et al.*, 2013).

*Cm*BVMO was purified from the soluble fraction of Syn_zia_BVMO extract. Since a His-tag was fused at the C-terminus of the protein, its recovery was made possible by an Immobilized Metal-ion Affinity Chromatography (IMAC). Elution of the loaded resin was achieved by an imidazole solution, and then the protein-rich eluted fraction was cleaned from imidazole with a de-salting procedure.

The direct activity assay is based on the absorbance properties of NADPH in contrast to those of $NADP^+$. In fact, NADPH has an absorbance peak at 340 nm, whereas $NADP^+$ shows no absorbance at this wavelength. The decrease in absorbance at 340 nm (A_{340}) is a direct measure of NADPH consumption. A reaction mix with NADPH and *Cm*BVMO was initially used as reference, since the enzyme can perform a small degree of "uncoupling reaction". This term refers to a basic activity of BVMOs in absence of a specific substrate, in which molecular oxygen is reduced to hydrogen peroxide (Torres Pazmiño *et al.*, 2008). A_{340} was checked over time, before and after the addition of 3-nonanone. The resulting immediate change of slope (Fig. 13) denotes an increase in NADPH consumption, and thus in enzymatic activity.
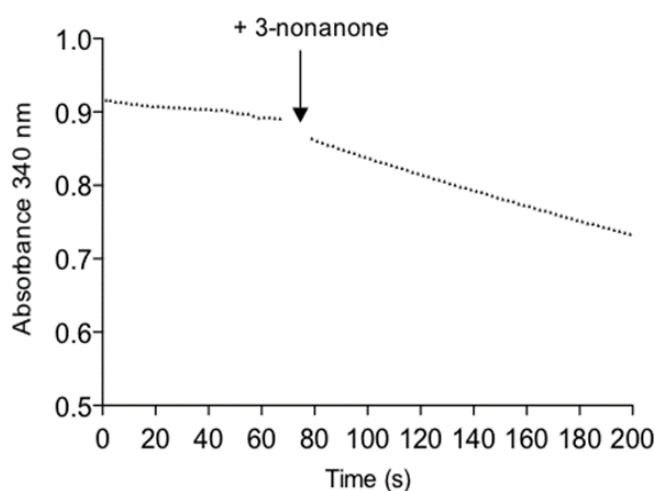

Figure 13: NADPH absorbance at 340 nm over time, for the check of enzymatic activity. The addition of 3-nonanone is indicated.

For the native-PAGE, a native gel was prepared. Native gels are particular polyacrylamide gels whose main purpose is to keep the migrated proteins in their native conformation to preserve their activity. Hence, no denaturing or reducing agent was added. In this case, the separation during electrophoresis is given by the isoelectric point (pI) of each protein. Since pI values are usually very similar between proteins, an acrylamide gradient is suggested to better separate the bands. In particular, a 4%-12% and a 4%-20% gradient have been used in this experiment.

The colorimetric assay consists of performing the enzymatic reaction of the desired protein after the electrophoresis in the native gel. The visualization of the reaction is granted by a chromogenic substrate, which in this case is nitro blue tetrazolium (NBT). This salt is pale yellow and soluble when oxidized, while becomes purple-blue and insoluble when reduced. Considering the BVMO reaction (see par 2.2), it works as final electron acceptor, instead of the oxygen atom. Thus, in practical terms, incubation of the migrated samples with NADPH, NBT and a well-accepted substrate, should reveal the activity of *Cm*BVMO.

Samples of wt and Syn_zia_BVMO were taken at day 3 of mixotrophic cultures in standard conditions and processed for protein extraction. After the electrophoresis, the lanes were separated to apply different treatments: (1) incubation with NADPH, 3-nonanone and NBT; (2) incubation with NADPH and NBT, without the substrate. The first treatment was used to check the BVMO activity, while the second was necessary to check for aspecific activity of other enzymes (f.i. NADPH-dehydrogenase). The result is reported in Figure 14.
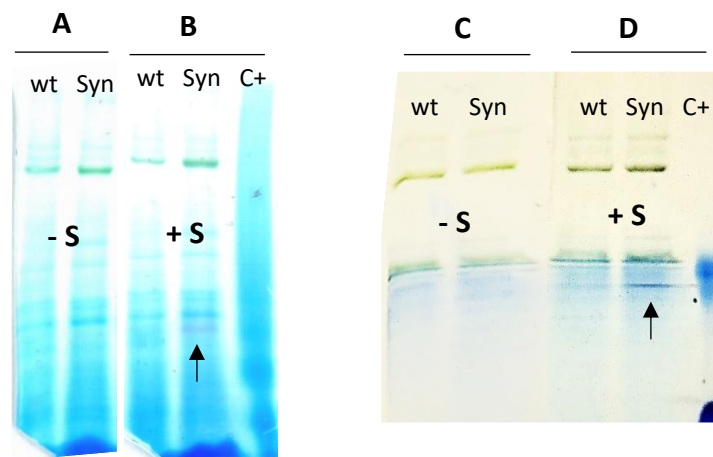

Figure 14: Native PAGE of total protein extracts of wt and Syn_zia_BVMO. Bands resulting from the NBT activity assay are indicated with arrows. Wt: wild type strain. Syn: Syn_zia_BVMO strain. C+: purified CmBVMO. -S: Incubation without the substrate. +S: Incubation with the substrate. No molecular weight marker is present due to unavailability of non-denaturing markers.

In both the gradients (4%-12% and 4%-20%) a single purple-blue band appeared in the Syn strain extract in presence of 3-nonanone (Fig. 14 B, D), whereas no bands were detected in absence of 3-nonanone (Fig. 14 A, C). Moreover, in the wt strain extract no bands were visible, in none of the conditions tested. Unfortunately, the positive control in the last lane, i.e. purified *Cm*BVMO, resulted in an aberrant migration and did not show in-gel activity.

Despite the absence of a positive control, an enzymatic activity towards 3-nonanone was detected in Syn cell extract, whereas no activity was revealed in the negative control (wt strain).

4.2 Possible involvement of *Cm*BVMO in unbalancing the NADPH/NADP⁺ ratio

In the first part of this work, the Syn_zia_BVMO strain showed a prolonged growth and an increased biomass accumulation compared to the wild type. The observed phenotype was hypothesized to be related with the expression of the heterologous enzyme *Cm*BVMO in an active form. Hence, the study moved on to the search of the possible causes of this peculiar phenotype, in relation to the activity of the recombinant enzyme.

As said, BVMOs require a redox cofactor, which in the case of *Cm*BVMO is NADPH. This essential reducing equivalent is generated in *Synechocystis* cells during the light reactions of photosynthesis, together with ATP. Both NADPH and ATP are then consumed, during dark reactions, by the Calvin cycle for CO_2 reduction in organic compounds. Theoretical analysis showed that light reactions generate 2.57 ATP/2 NADPH while dark reactions require 3 ATP/2 NADPH (Kramer and Evans, 2011; Marcus *et al.*, 2011). Therefore, the ATP generated in the light reactions is insufficient to meet the energy requirement for CO_2 fixation, and thus limits photosynthetic efficiency. Recently, Zhou and co-workers have formulated an interesting hypothesis about this limitation (Zhou *et al.*, 2016). They argued that, to fulfil the demand of ATP, light reactions should generate 3 ATP every 2.33 NADPH molecules. However, this would result in a NADPH imbalance, since only 2 NADPH will be consumed in dark reactions. Thus, increasing consumption of this cofactor might improve the coupling between light and dark reactions, increasing photosynthetic efficiency. In their work, this hypothesis was been tested by introducing a NADPH-consuming enzyme in *Synechocystis* sp. PCC 6803 (Fig. 15), together with other two non-redox enzymes. The resulting engineered strain showed a significant increase in cell growth rate, dry cell weight, CO_2 fixation and photosynthetic efficiency (Zhou *et al.*, 2016). Their hypothesis seems thus sufficiently demonstrated.
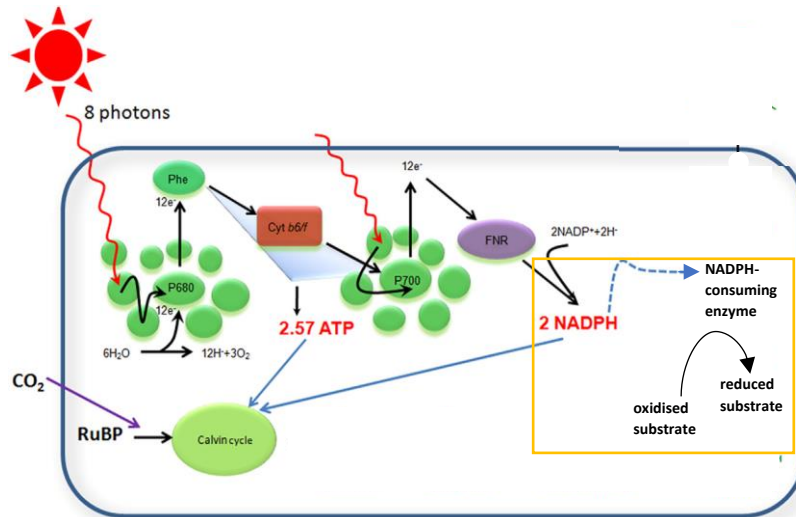
Figure 15: Diagram of ATP and related NADPH production in the light reactions, with the addition of the NADPH-consuming enzyme. Image from Zhou et al., 2016.

The extrapolation of these conclusions to the present work are intriguing. The increased growth of the Syn_zia_BVMO strain may be explained by an induced extra NADPH consumption, which in turn may lead to an increased photosynthetic efficiency.

To verify this hypothesis, several analysis were carried out on the wt and recombinant strain.

4.2.1 Oxygen evolution and respiration

At the beginning of the light reactions of photosynthesis, the energy derived from photon absorption is used to oxidise water molecules. The process is called water splitting, since H_2O is divided into protons and molecular oxygen, and takes place in the oxygen-evolving complex (OEC). This implies that the rate of photosynthesis is directly proportional to O_2 generation. Since it is a gas, O_2 can freely diffuse outside the cells, and can be quantified with dedicated instruments. To sum up, measuring oxygen evolution rate is a possible way to quantify photosynthetic rate, and so efficiency. In the aforesaid hypothesis, NADPH consumption should lead to a higher photosynthetic efficiency. Measuring O_2 evolution rate of the recombinant strain should give some hints about the plausibility of this hypothesis.

For O_2 quantification, an oxygen electrode was employed. Since oxygen is consumed by respiration, to obtain the total amount of produced O_2 by photosynthesis the measures were performed in two conditions. A first measure, in the absence of light, allowed to retrieve the respiration rate, a second measure, in saturating light, allowed to retrieve the oxygen evolution due to the combination of photosynthesis and respiration. The total quantity of oxygen produced by

photosynthesis could be deduced as the difference of the previous two measures (Genty, Briantais and Baker, 1989).

Then, the values of oxygen evolution were normalized. In fact, there may be a high variability between cells in terms of number of OECs. The chlorophyll content of a sample is related to its number of OECs by a precise invariant stoichiometry (~38 Chl/OEC) (Tang and Diner, 1994), therefore it can be used to normalize the oxygen evolution rate of the samples. Chlorophylls can be easily extracted with organic solvents and quantified via absorbance at the 680-nm peak. Following normalization, the results were expressed in µmol O_2/mg Chl/h.

In this work, oxygen evolution experiments were conducted on wt and recombinant *Synechocystis* cells, cultured in liquid in mixotrophic standard conditions. Measures of oxygen evolution and respiration, as well as chlorophyll quantification, were performed at day 4, 8 and 16. In these three days, differences in OD were, respectively, 0, 2 and 5.5 units. The results show that the oxygen evolution rate for the Syn_zia_BVMO is higher than the one of wt in all the three days considered (Fig. 16). The higher difference between the two strains is visible at day 8, in which O_2 evolution of Syn_zia_BVMO is 6-fold higher than the wt one.
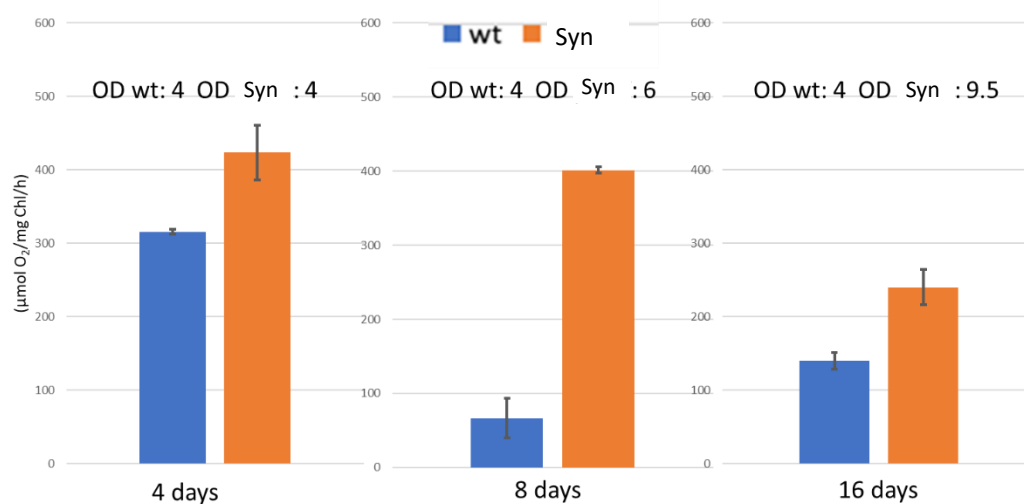

Figure 16: Oxygen evolution of wt and Syn_zia_BVMO strain, at day 4, 8 and 16 of mixotrophic cultures. The values reported are means of three independent experiments, with relative standard error bars.

4.2.2 PHB accumulation during nitrogen starvation

Synechocystis and some other cyanobacterial species can accumulate polyhydroxibutirate (PHB) polymers when subjected to phosphorous or nitrogen starvation (Panda *et al.*, 2006). This phenomenon has been recently correlated to the redox state of the cells (Hauf *et al.*, 2013). In fact, lack of nitrogen hampers aminoacids synthesis, and consequently also the TCA cycle, which is the main sink of NADPH. As a result, reducing equivalents and fixed carbon start to accumulate, severely compromising cellular metabolism. Biosynthesis of PHB (Fig. 18) is thus an essential NADPH and carbon-sink, alongside with the synthesis of other metabolites like sorbitol and glycogen (Hauf *et al.*, 2013). Moreover, phycobiliproteins are degraded to recover their great amount of nitrogen atoms (Collier and Grossman, 1994). In this way, cells are able to cope with nutrients-limited situations.
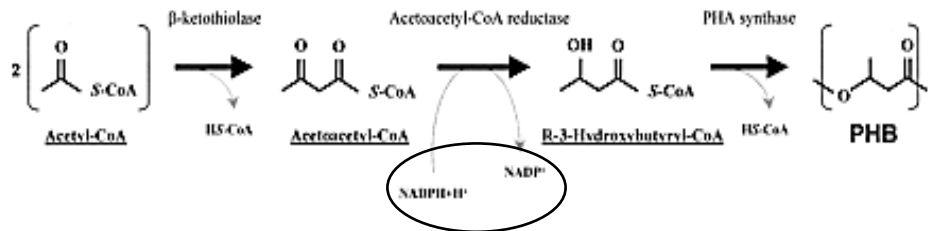

Figure 18: Schematic overview of PHA synthesis and the involved enzymes. Image from Taroncher-Oldenburg et al., 2000.

It can be inferred from these observation that the extent of PHB accumulation is directly proportional to the NADPH content of cells (Hauf *et al.*, 2013). In the context of this work, the NADPH consumption given by the BVMO activity should result in a decreased NADPH level, compared to wt cells. If nitrogen starvation is applied, the final result should be a decreased content in PHB. Since PHB polymers can specifically be stained with a hydrophobic fluorescent dye (Nile Red), they can be easily quantified in vivo without any extraction or purification.

Therefore, nitrogen-starved cultures of the wt and recombinant strains were set, in order to quantify their PHB content. The nitrogen limitation has been applied to mixotrophic cultures of the two strains. These cultures were pelleted and resuspended in nitrogen-less BG11 medium after 1 day of growth in standard conditions. Na-acetate was added to enhance PHB accumulation, as previously reported (A. K. Singh *et al.*, 2017). Samples of the cultures were also collected to analyse pigment content of the cells, before (day 0) and after (day 12) the onset of nitrogen starvation. The absorbance spectra (Fig. 19) of the total pigments show a general decrease in quantity during N starvation. As expected, the almost complete disappearance of the 620-nm phycobiliproteins peak confirms their dismantling and the reutilization of their N atoms. For the PHB quantification, after the resuspension in N-less BG11 five samples were collected in different days and stained with Nile red. The related fluorescence was then quantified via a fluorescence spectrophotometer, and then normalized on the number of cells. The

values obtained (Fig. 20) are higher for the wt in all the 5 days. Both indirect measurements (phycobilisomes degradation and relative amounts of PHB) suggest that the NADPH level in the Syn_zia_BVMO strain may be intrinsically lower.
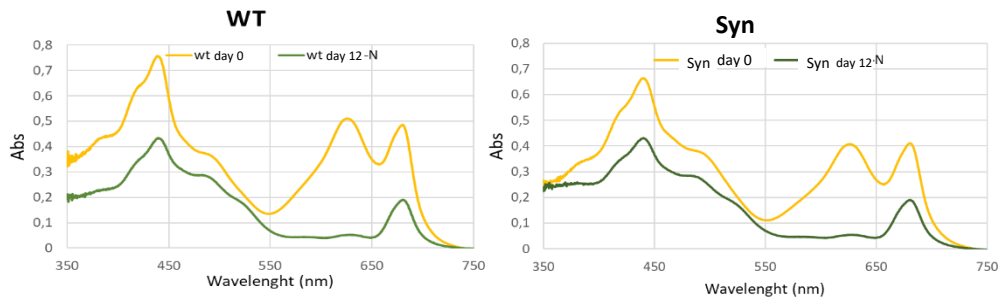

Figure 19: Absorbance spectra of total extracted pigments of wt and Syn_zia_BVMO, measured before nitrogen starvation (day 0) and some time after (day 12) the application of nitrogen starvation.

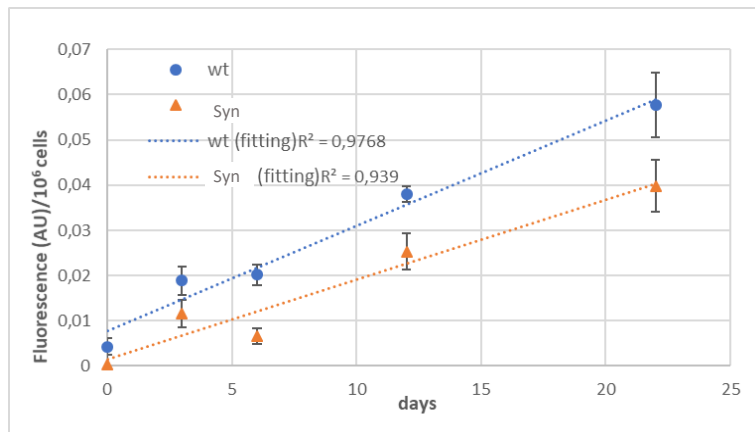*Figure 20: Spectroscopic quantification of Nile red fluorescence in nitrogen-straved wt and recombinant strains. The values reported are means of three independent experiments, with relative standard error bars.*
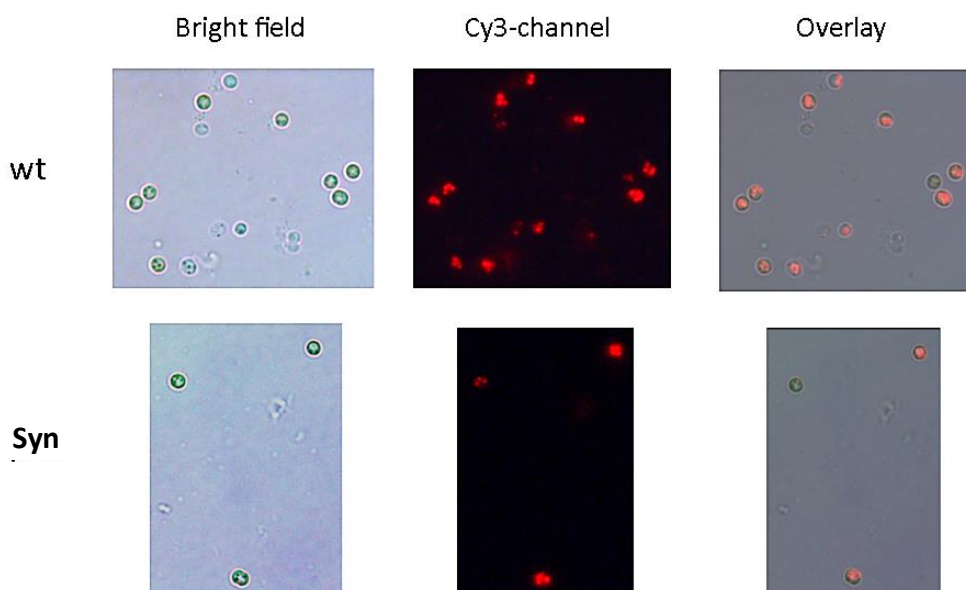

Figure 21: Fluorescence microscopy images of wt and Syn_zia_BVMO stained with Nile red. The overlay is the superposition of the bright field image and the Cy3-channel (for Nile red) one.

Visualization of PHB granules was checked by fluorescence microscopy in cells from the last sampling (day 22). Images in bright field and with the proper fluorescence filter were collected. In Figure 21 an example is presented for each strain. **The PHB granules are clearly visible in both the strains, confirming the induction of PHB synthesis.**

4.3 Looking for a possible substrate of *Cm*BVMO in *Synechocystis* cells

The essential requirements for the activity of CmBVMO in the recombinant strain are NADPH and substrates. Previous experiments focused on NADPH consumption, but still no evidences had been gathered about the possible *in vivo* substrates of CmBVMO. Given the substrate specificity of this enzyme (see par. 2.2.1), suitable ketones/aldehydes have been searched throughout the metabolic pathways of *Synechocystis* which are reported in literature. Eventually, a promising substrate was found in the fatty acids pathway.

In the fatty acids biosynthetic pathway, malonyl-CoA units are assembled to form long aliphatic chains. The main final product is hexadecanoyl-ACP, which follows two main different paths in *Synechocystis*. It can be diverted into fatty acids production or into alkane biosynthesis (Fig. 22). In this second pathway, one of the intermediates is a long-chain fatty aldehyde, hexadecanal, produced by the enzyme fatty acyl-ACP reductase (FAR; gene *sll0209*). Looking at the substrate scope of
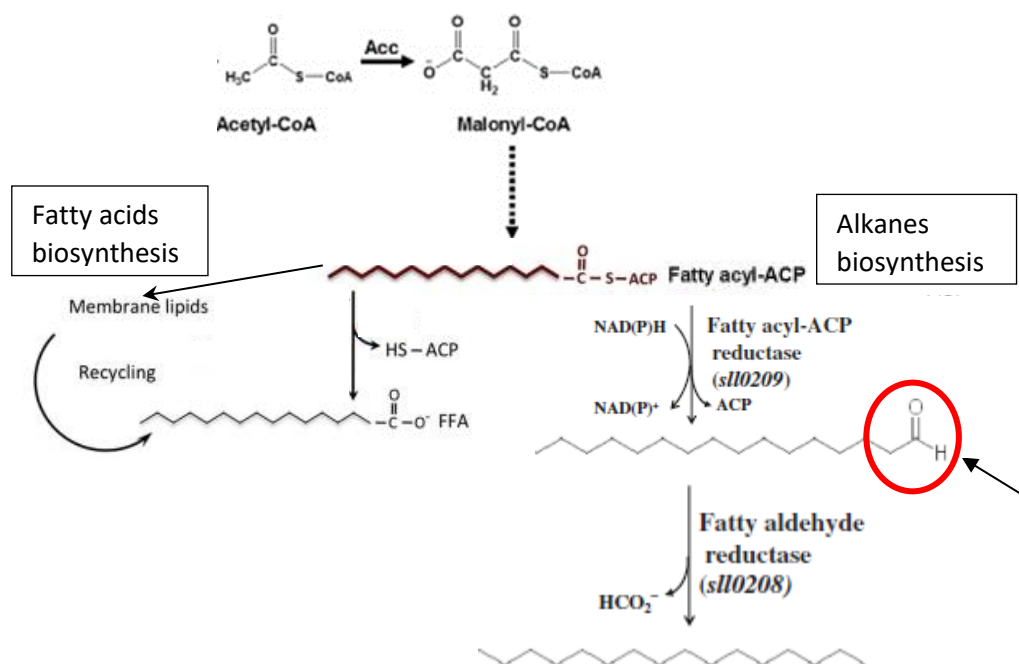

Figure 22: Schematic view of alkane biosynthesis pathways in Synechocystis sp. PCC 6803. The red circle indicates the aldehydic group of the fatty aldehyde.

CmBVMO (see par.2.2.1), this aldehyde could be a possible substrate of the enzyme. This hypothesis was thus tested.

4.3.1 Activity of CmBVMO with hexadecanal as substrate

Since only medium-chain fatty aldehydes had been tested for the characterization of *Cm*BVMO (see par. 2.2.1), the activity towards long-chain fatty aldehydes, like hexadecanal, was verified. The activity assay was carried out as previously described and the rate of NADPH consumption was monitored at the spectrophotometer (see par. 4.1.4). First, the possibility of a spontaneous reaction between hexadecanal and NADPH was checked, and proved to be absent, since NADPH was not consumed (Fig. 23 A). A reaction mix with only NADPH and *Cm*BVMO was used as reference, due to the occurrence of the uncoupling reaction (Fig. 23 B; see par. 4.1.5).

The graph in Fig. 23 C represents the NADPH consumption of *Cm*BVMO in presence of hexadecanal. After the subtraction of the uncoupling rate, the calculated enzymatic activity was 0,041 U/mg. Since hexadecanal is a very low soluble compound in aqueous buffer, it was added at a concentration of 1,25 mM in the enzymatic assay, reaching its solubility limit. Despite this low concentration, *Cm*BVMO resulted active, showing an enzymatic activity similar to other more soluble substrates (f.i. 2-octanone 10 mM: 0,092 U/mg).

The same substrate was used for a small-scale biotransformation and the final product of the reaction was analysed by gas chromatography-mass spectrometry (GC-MS).

The biotransformation was prepared with hexadecanal, NADP+, the enzyme *Cm*BVMO, glucose and glucose dehydrogenase (GDH). GDH with an excess of glucose was used as NADPH-regenerating system, a common method to avoid stoichiometric use of NADPH. The same mixture without *Cm*BVMO was used as negative control. Both the reaction mixture and the control were incubated over night and then processed for the GC-MS. The results show the appearance of a new peak in the chromatographic profile of the reaction mix with *Cm*BVMO (Fig. 24 B), in comparison to the one of the control (Fig. 24 A). MS analysis of the reaction mixture with the enzyme showed a different profile compared to the control (Fig. 24 C, D). These results indicate that hexadecanal was converted into a new product in the reaction catalysed by *Cm*BVMO.
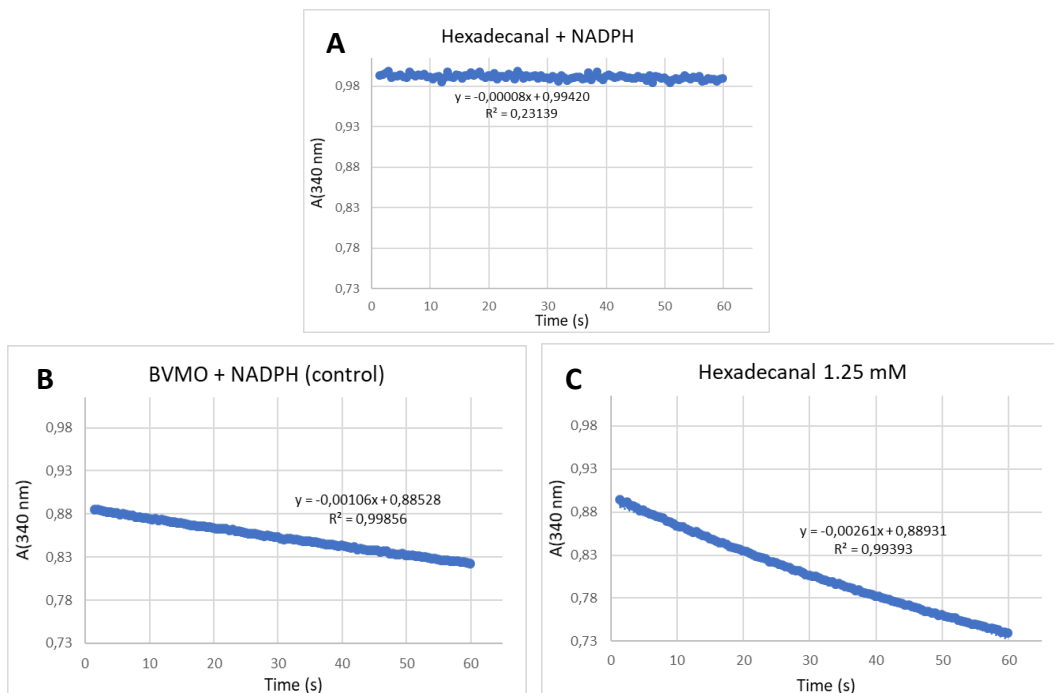
Figure 23: Enzymatic activity assay through NADPH absorbance measures. *A*: Hexadecanal and NADPH. *B*: control reaction with CmBVMO and NADPH. *C*: Reaction with CmBVMO, NADPH and 1.25 mM hexadecanal. The slope of each graph is the angular coefficient of the reported equations.
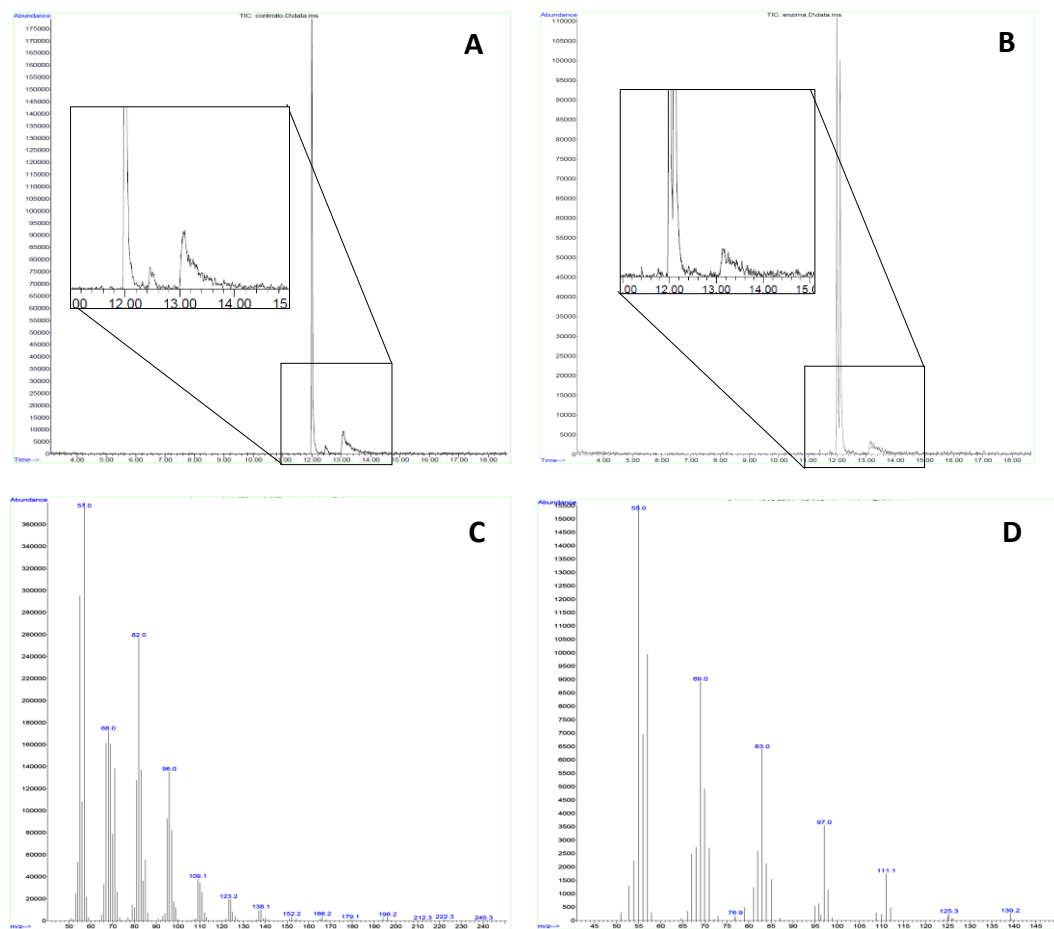
Figure 24: GC-MS analysis of the reaction mix without (*A,C*) and with CmBVMO (*B,D*).
A,B: Gas chromatography profiles. *C,D*: Mass spectrometry spectra. The appearance of a new peak in *B* is highlighted. In *D*, the most intense peaks are different from those in *C*.

4.3.2 Knockout strains for the *sll0209* locus

To evaluate the possible involvement of these fatty aldehydes as substrates for *Cm*BVMO, it was decided to knock-out the *sll0209* locus in both the wt and Syn_zia_BVMO strain. The *sll0209* locus refers to the gene encoding the fatty acyl-ACP reductase. The knock-out of this gene would prevent the formation of the corresponding aldehyde in the mutant strains. If hexadecanal is really consumed by *Cm*BVMO *in vivo*, this mutation should result in the inactivity of the enzyme and thus loss of the observed phenotype.

Since *Synechocystis* is naturally prone to homologous recombination, the mutagenic constructs were provided with specific genomic sequences to target the recombination. Two 400-bp-long sequences (FR1 and FR2), matching exactly the *sll0209* flanking regions, were amplified and cloned in a vector plasmid (pBSK-, see Materials and Methods). A chloramphenicol resistance cassette (Cm^R) was inserted in-between the *sll0209* flanking regions in order to disrupt the corresponding gene in the strain expressing the *Cm*BVMO. In this way, a great part of the *sll0209* gene will be deleted. The resulting mutant strain would have two resistance cassettes: the one conferring kanamycin resistance (Kan^R), previously used to select Syn_zia_BVMO strain, and a second conferring chloramphenicol resistance, for the selection of the *sll0209* knock-out.

In order to compare the growth profile of the new mutant strain with a proper control, the wild-type strain of *Synechocystis* was mutated in the same locus *sll0209*, inserting both the kanamycin and chloramphenicol cassettes. In this way, the metabolic load of the two strains to be compared could be considered equal (apart from the absence or presence of the *Cm*BVMO enzyme).

Given the considerable dimensions of the Cm^R+Kan^R construct (~3000 bp), the possible difficulty in obtaining the desired recombination event was taken into account. Thus, the wt strain was also transformed with the Cm^R construct.

After transformation, cells were plated on BG11 solid medium supplemented with the proper antibiotic, at a concentration of 10 µg/ml. Single colonies were picked and transferred to plates containing 25 µg/ml of antibiotic(s), then six subcloning passages were performed in agar plates containing 50 µg/ml of antibiotic(s). This procedure, already described for the construction of the Syn_zia_BVMO strain (see par. 2.3), is required to ensure homoplasmy.

The selected strains with the corresponding genotype are summarized in Table 1. From the plates containing 10 µg/ml of antibiotic(s), two independent clones were picked for Δ(sll0209)_(CmR+KanR) and for SynΔ(sll0209), while three independent clones were picked for Δ(sll0209)_(CmR).

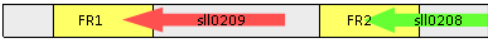| Mutant [Clones]	Genotype	Scheme of *sll0209* locus
		Wild type:
Δ(*sll0209*)_(Cm^R+Kan^R) [clone 1 and 2]	KO mutant for *sll0209*, Kan and Cm resistance	
Δ(*sll0209*)_(Cm^R) [clone 3,4 and 5]	KO mutant for *sll0209*, Cm resistance	
Syn Δ(*sll0209*) [clone 6 and 7]	KO mutant for *sll0209*, BVMO-expressing strain, Kan and Cm resistance	

Table 1: Knock-out strains with corresponding genotype and scheme of sll0209 locus. The clones indicated are independent transformants from the plates with 10 μg/ml of antibiotic(s).

Homoplasmy in the selected clones was verified by PCR. A first PCR, using a locus-specific primer (FR1 or FR2) and a Cm^R- or Kan^R-specific primer, confirmed the right insertion of the recombinant construct in all the clones (Fig. 25). Moreover, it confirmed that the transformation of wt with Cm^R+Kan^R had been successful; hence, Δ(*sll0209*)_(Cm^R) clones were not further used.
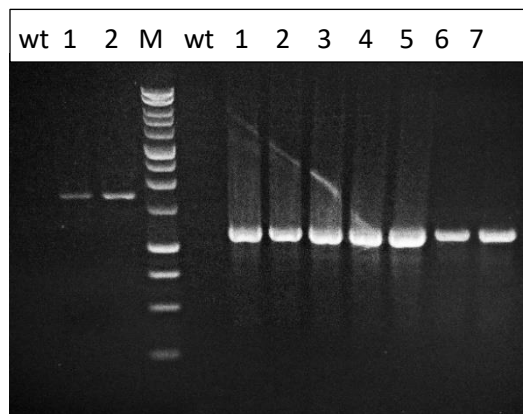
Figure 25: Agarose gel electrophoresis of PCR products. Left side: amplicons obtained with locus-specific primer FR1 and Kan^R-specific primer. Right side: amplicons obtained with locus-specific primer FR2 and Cm^R-specific primer. Clones are indicated with the respective number. Wt: amplicons from wild type genome. M: DNA marker.

A second PCR with the two locus-specific primers was sufficient to confirm homoplasmy for Δ(*sll0209*)_(Cm^R+Kan^R), since the inserted construct gave longer amplicons than the wt ones. SynΔ(*sll0209*) showed amplicons comparable in length to the one obtained for the wt locus (Fig. 26 A). These amplicons were thus cut using the endonuclease NcoI, whose restriction site is present only in the mutated construct. The result showed the complete absence of uncut bands, finally confirming homoplasmy also for SynΔ(*sll0209*) (Fig. 26B). Hereafter, the Δ(*sll0209*)_(Cm^R+Kan^R) mutant will be called "Δ*sll0209*" and the SynΔ(*sll0209*) mutant will be called "SynΔ*sll0209*".
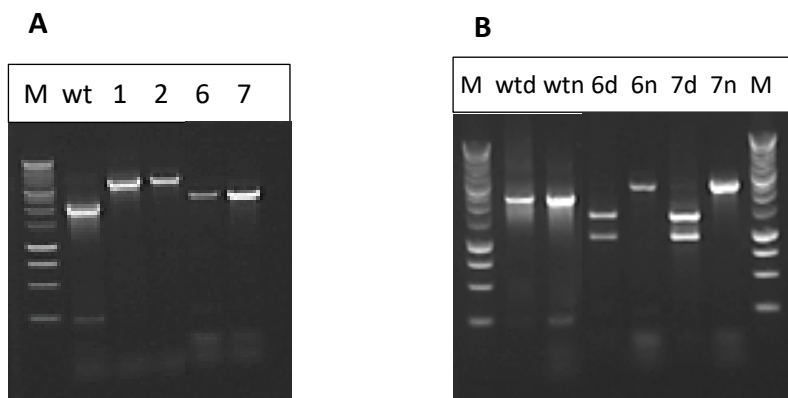
Figure 26: Agarose gel electrophoresis of PCR products (A) and digested PCR products (B). A: amplicons obtained with locus-specific primers FR1 and FR2. Clones are indicated with the respective number. B: Digested amplicons. Letter "d" after the clone number indicates digested samples, while letter "n" indicates non-digested samples. Wt: amplicons from wild type genome. M: DNA marker.

4.3.3 Growth profiles of the *Δsll0209* mutants

The first characterization of the new mutants went through monitoring of the growth curves. Standard conditions in mixotrophy were applied. The graph in Fig. 27 A reports the growth curves of all the clones of each mutant. Comparison with the wt and Syn_zia_BVMO growth curves (Fig. 27 B; see par. 4.1.1) indicates that all the mutant strains show a growth profile equal to or slightly slower than the wt. This is true also for the Syn*Δsll0209* clones, which grow similarly to *Δsll0209* ones. The almost complete absence of the prolonged-growth phenotype is thus an initial indication, which supports the identification of the selected aldehyde as the sought *Cm*BVMO substrate.
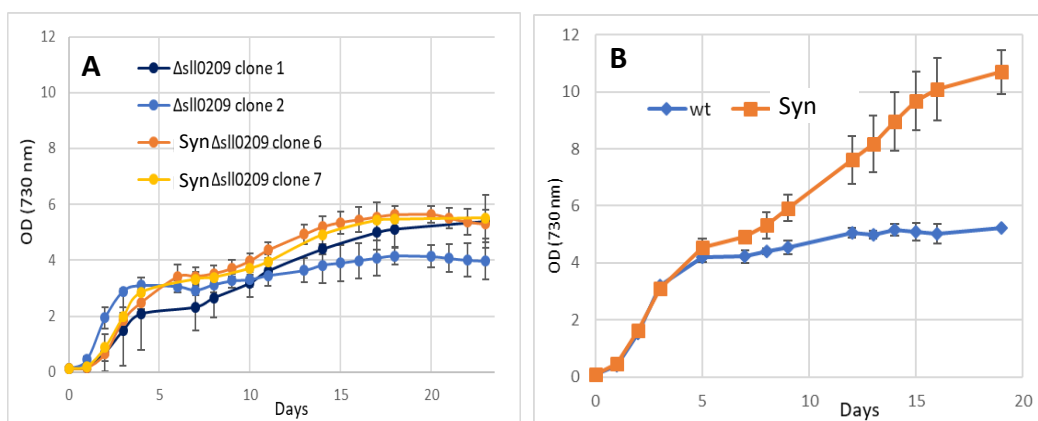
Figure 27: Growth profiles in standard mixotrophic conditions of Δsll0209 and SynΔsll0209 (A) and of wt and Syn_zia_BVMO strains (B). The values reported are means of three independent experiments, with relative standard error bars.

4.3.4 PHB quantification of the mutant strains

If the activity of *Cm*BVMO in the Syn*Δsll0209* is hampered by the absence of its substrate, the enzyme wouldn't be able to consume NADPH. Thus, NADPH levels should be more or less equal to those of *Δsll0209*. To verify this, PHB in both the newly engineered strains were quantified as described previously (see par. 4.2.3). Nitrogen starvation was applied after one day of standard mixotrophic growth, and the fluorescence measures were done after 5 and 11 days. The results (Fig. 28) show a lower fluorescence in the Syn*Δsll0209*, in comparison to *Δsll0209*. These results indicate that the BVMO activity seems to influence the formation of PHB also in the knockout mutant. Therefore, the lower content of PHB in the strains expressing the BVMO may not be related to the presence of the substrate hexadecanal. During the nitrogen-starving condition other substrates may become available for the BVMO activity.
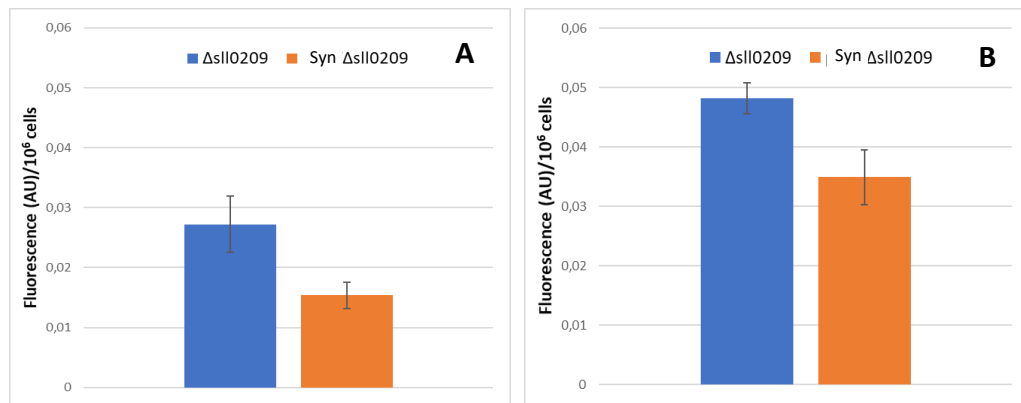
Figure 28: Spectroscopic quantification of Nile red fluorescence in nitrogen-starved cultures of Δsll0209 and SynΔsll0209, at day 5 (A) and 11(B). The values reported are means of three independent experiments, with relative standard error bars.

5. Discussion

The aim of the present work was the characterization of Syn_zia_BVMO, a *Synechocystis* sp. PCC 6803 strain expressing the BVMO enzyme from *Cyanidioschyzon merolae*. The study started with the verification of the expression of the heterologous enzyme in *Synechocystis* cells by mRNA and Western blot analysis. These analyses highlighted the leakiness of the ziaA promoter, inducible by zinc. In fact, *Cm*BVMO transcript and protein were detected also in non-induced cells, even if in a lower quantity with respect to the cells grown in standard condition ($1,3 \ \mu M \ Zn^{2+}$ BG11 medium) or induced by zinc ($5,3 \ \mu M \ Zn^{2+}$).

To check for eventual toxic effects of *Cm*BVMO, the growth profile of the recombinant strain was analysed. Surprisingly, this strain showed a longer growth phase in comparison to the wild-type. In particular, the Syn strain continued growing even when the wt strain had already entered the stationary phase, thus achieving higher cell densities. When the Syn strain reached its stationary phase, the OD value was almost twice the wt one. This phenotype was present both in mixotrophic and autotrophic conditions. Dry cell weight evaluation confirmed that the Syn strain could accumulate more biomass, reaching a 2-fold biomass formation after 15 days. TEM microscopy images showed no visible alterations, neither in shape nor in number of internal cell components. The enzymatic activity of *Cm*BVMO produced in *Synechocystis* was confirmed with an *in vitro* assay on the purified enzyme and with a native-PAGE of total extracts, followed by a colorimetric assay These data reasonably suggested that the enhanced growth of Syn_zia_BVMO is due to the activity of the *Cm*BVMO.

Consequently, by assuming that the effects of this enzyme on the cellular metabolism were primarily attributable to its catalytic activity, which encompasses the use of NADPH as cofactor, the following step was that of looking for a possible substrate. In this context, Zhou and co-workers provided a possible explanation. They were able to demonstrate that extra NADPH consumption increases the rate of electron transport along the photosynthetic chain, enabling higher ATP production and thus biomass accumulation (Zhou *et al.*, 2016). In our case, the measures of oxygen evolution rate, which is directly correlated to photosynthetic efficiency (Genty, Briantais and Baker, 1989), agree with this hypothesis, since the Syn strain produces more oxygen than the wt. This fact was observed in all the samples, taken at different days along the observed period of growth. Moreover, the recombinant strain showed a lower PHB accumulation, and this could be related to a lower NADPH level, as reported in literature (Panda and Mallick, 2007; Hauf *et al.*, 2013). In turn, this was considered a second indication of *Cm*BVMO activity. However, more evidences should be collected about the photosynthetic efficiency of the Syn strain, f.i. by measuring quantum efficiency of the photosystems II and I. According to this possible mechanism (i.e. higher photosynthetic efficiency stimulated by increased consumption of NADPH), the absence of the phenotype in high light can also be explained. In fact, during high

light stress, photoprotection mechanisms, like ROS scavenging and biosynthesis of photoprotective pigments, are activated and require a higher consumption of energy and redox power (Singh *et al.*, 2008). In this condition, therefore, more NADPH is consumed by the endogenous enzymes and is possibly subtracted to the heterologous *Cm*BVMO, hampering its activity. Also in this case, other experiments are required to verify the formulated hypothesis (f.i. NADPH and ATP direct quantification).

The NADPH consumption by *Cm*BVMO should be necessarily driven by the conversion of a specific substrate, or more than one, into an oxygenated product. Among all the metabolites in *Synechocystis*, the fatty aldehydes (mainly hexadecanals and octadecanals) from the alkane biosynthetic pathway were considered compatible molecules. They have an aldehydic group in C1, they are linear and unsaturated, and thus they resemble the substrates preferred by *Cm*BVMO, as derived by its former biocatalytic characterization (Beneventi *et al.*, 2013). The activity of the enzyme towards hexadecanal was successfully proven *in vitro*.

To assess the role of this molecule as substrate of *Cm*BVMO, knock-out mutant strains for the *sll0209* locus were produced. This locus encodes for the enzyme responsible for hexadecanal production from acyl-ACP (FAR, fatty acyl-ACP reductase). The growth curve registered for this mutant Syn∆*sll0209* shows the almost complete abolition of the phenotype observed for Syn_zia_BVMO. Therefore, from these preliminary analysis, the prolonged growth phenotype observed in Syn_zia_BVMO strain seems to be due to the *Cm*BVMO activity on hexadecanal with the consequent consumption of NADPH (as already explained). Other hypotheses, however, as a direct influence of the oxidized hexadecanal on *Synechocystis* metabolism, cannot be excluded. A strong proof for this hypothesis could be given by a compared metabolomic analysis of Syn and Syn∆*sll0209*, focusing on the possible products of *Cm*BVMO. A standard Baeyer-Villiger reaction on hexadecanal would produce hexadecyl formate, hence this molecule should be detected in Syn and not in Syn∆*sll0209*. However, it has been observed that formate esters, generated from aldehydes by BVMOs, quickly auto-hydrolyse to the respective alcohol derivatives (Kamerbeek *et al.*, 2003; Moonen *et al.*, 2005; Bisagni *et al.*, 2014). For instance, a recent work showed that alkyl formates esters generated *in vitro* by the BVMO from *Aspergillus flavus* underwent spontaneous hydrolysis, generating formates (HCOO⁻) and fatty alcohols (Ferroni *et al.*, 2017) (Fig. 29 A).
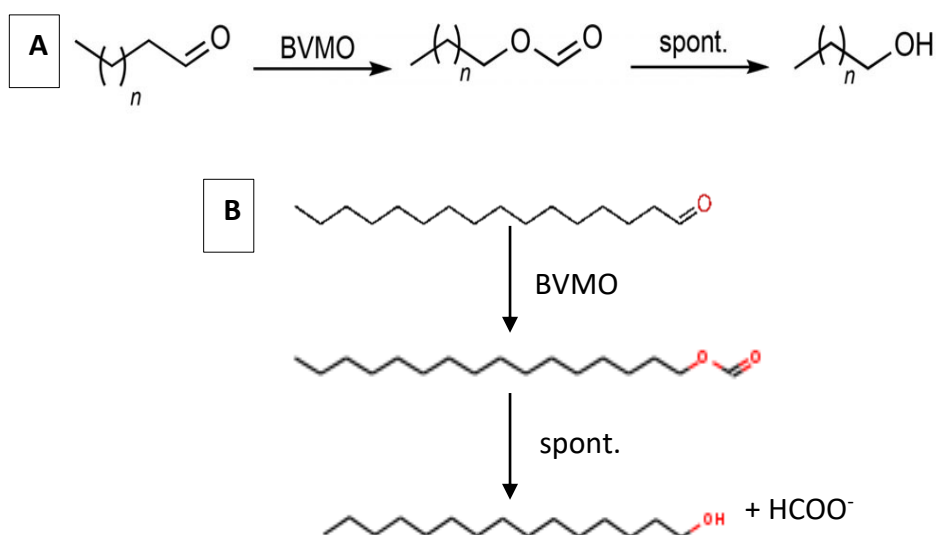
Figure 29: Schematic representation of BVMO reaction followed by spontaneous hydrolysis of the resulting alkyl formate to fatty alcohol. A: General scheme proposed by Ferroni et al. 2017. B: Specific scheme for hexadecanal, converted to hexadecyl formate and then evolving to pentadecanol.

If this is the case also for the product of the *Cm*BVMO expressed in *Synechocystis*, the hexadecyl- and octadecyl-formate would give rise to pentadecanol and heptadecanol, respectively (Fig. 29 B). A GC-MS analysis, with a fatty alcohol and an alkyl formate as internal standards, would be useful in determining the presence in the Syn strain of the alcohol and/or formate derivatives. Since *Synechocystis* doesn't produce fatty alcohols, their presence would be a strong evidence supporting the spontaneous hydrolysis of the alkyl formate ester. In this scenario, also formate production from the hydrolysis should be taken into account. Both the fatty alcohol(s) and $HCOO^-$ might give an important contribution to the prolonged-growth phenotype that we have observed.

6. Conclusions and perspectives

Finally, the peculiar phenotype of Syn_zia_BVMO makes the use of this strain advantageous for biocatalysis purposes, since overall productivity is dependent on biomass accumulation. This strain would be ideal for batch or semi-continuous production, because with these modes of operation the cell density of Syn is allowed to increase up to its maximum. In the presented growth curves, the highest OD reached by Syn was 11 units in mixotrophy after 20 days, and 13 units in autotrophy after 28 days. Thus, even though the growth in autotrophy is slightly slower, the culture can reach a higher cell density compared to mixotrophy. Moreover, growth in autotrophy is advantageous since no sugary feedstock is needed. Hence, this culture condition could be used for whole-cell biocatalysis with Syn strain.

Incubation of Syn cells with various substrates could result in the formation of exploitable products, and if these products are excreted in the medium, the production would result even more appealing and advantageous. Thus, membrane permeability will be an important parameter by which selecting the candidate substrates. Moreover, if the hypothetic hydrolysis of formate to alcohol will be proven and confirmed, the Syn strain would be exploitable by itself, since fatty alcohols could be recovered and used as biofuels or industrial additives.

7. Materials and Methods

7.1 Materials

7.1.1 Enzymes and reagents

All the chemical reagents were purchased by Sigma-Aldrich.

The enzyme used for all the polymerase chain reactions (PCRs) was GoTaq® (Promega).

The Bradford reagent used for the protein quantification was produced by Bio-Rad.

The primary polyclonal antibody anti-BVMO used for Western blot was produced in-house using a BVMO-immunised rabbit.

The secondary antibody (goat anti-rabbit, peroxidase conjugated) was purchased from KPL.

All the restrictions enzymes were purchased from New England Biolabs.

7.1.2 Oligonucleotides

SBVMO1f: CTACAACGACGGTTCACTAC

SBVMO1r: TAACCAGATTCCAGAGGGAC

SpetB1f: CCTTCGCCTCTGTCCAATAC

SpetB1r: TAGCATTACACCCACAACCC

Sll0209_for1 (locus-specific primer FR1): CAAGGCTGGCCAATAGATTAGAATG

Sll0209_rev2 (locus-specific primer FR2): TAACATATATATCCCTGTGGCGGAC

Sll0209_KO1rev: AGATAACTCGAGAGTACTGGAGCAGGCCAACA

Sll0209_KO2for:
CTGCAGCATATGAGATCTGGATCCGTCAGAATAAATAGGGGAAGG

Sll0209_KO3rev:
GGATCCAGATCTCATATGCTGCAGGCACTAATTTTTCCTGGGGCCG

Sll0209_KO4for: GCCGGAACTCTCGTAGCAGC

Clor1_rev: TATAGAATTCACATCTTGCGAATATATGTGTA

Kanam01_w: ATTAAATTCCAACATGGATGC

7.1.3 Plamids

- pBluescriptSK- (pBSK-) plasmid was purchased from Stratagene.
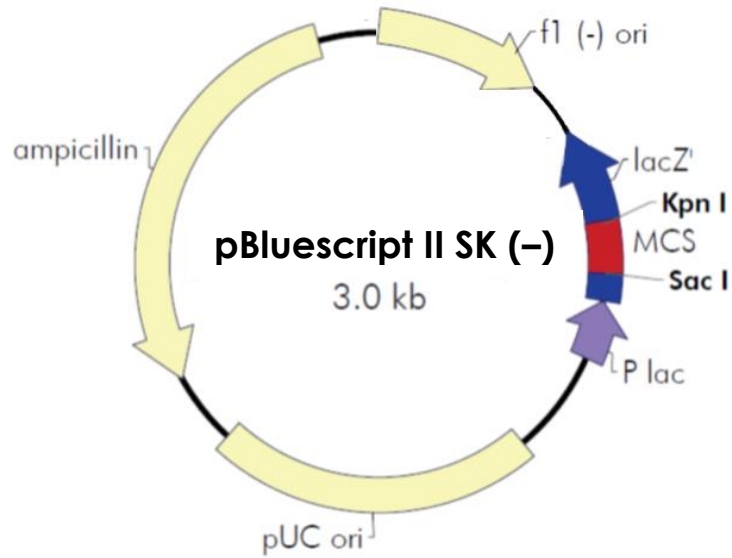
pBluescript II SK (+/–) Multiple Cloning Site Region

(sequence shown 598–826)
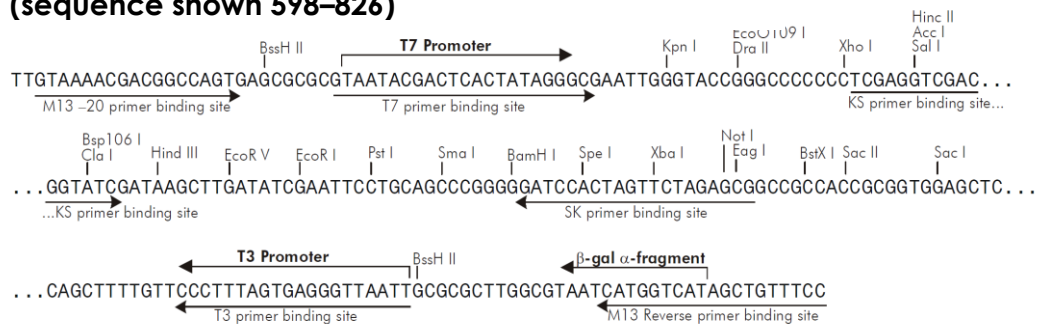
- pUC4K
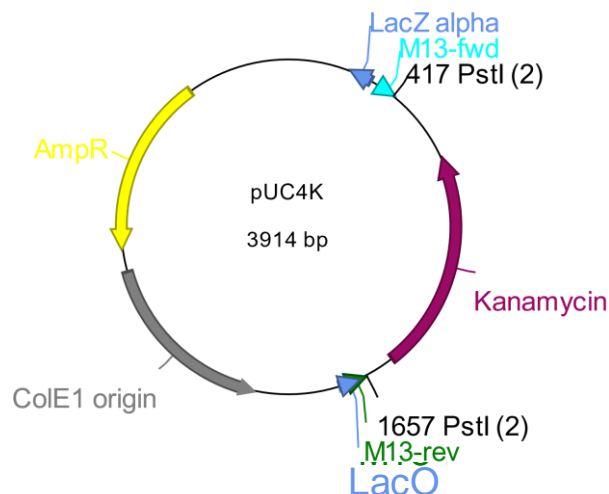
- pUC4CAT
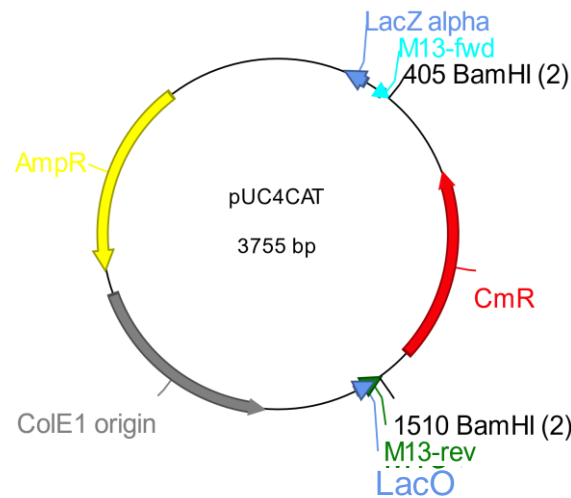
7.1.4 Instruments

Centrifuges: MIKRO 22 R Hettich zentrifugen; MPW-352R centrifuge.
Thermocycler: Eppendorf Mastercycle gradient.
Spectrophotometers: FullTech Instruments UV-1200, Agilent Cary UV-Vis.
Fluorescence spectrophotometer: Labsystems Fluoroskan Ascent FL
Beadbeater: Mini-beadbeater-24 Biospec Products.
DNA electrophoresis: Elettrofor chamber, Apelex ST500-D generator
Protein electrophoresis: Hoefer mini-vertical Gel Unit SE 260, Elettrofor generator
Scales: BEL engineering MARK 1000; Gibertini Crystal 100
pHmeter: Crison GLP 22
Oxygraph: Hansatech Oxygraph +; Lamp: Schott KL 1500

7.1.5 Strains of cyanobacteria and growth media

- *Synechocystis* sp. PCC 6803: wild-type strain.
- Syn_zia_BVMO: this strain derives from *Synechocystis* sp. PCC 6803. The ORF sequence *ssl0410* was substituted through homologous recombination with the expression cassette containing: the inducible promoter *ziaA*, the coding sequence for the Baeyer-Villiger monooxygenase of *Cyaniodioschyzon merolae* (BVMO), the kanamycin resistance gene (Kan^R).
  Scheme of the insertion given below.
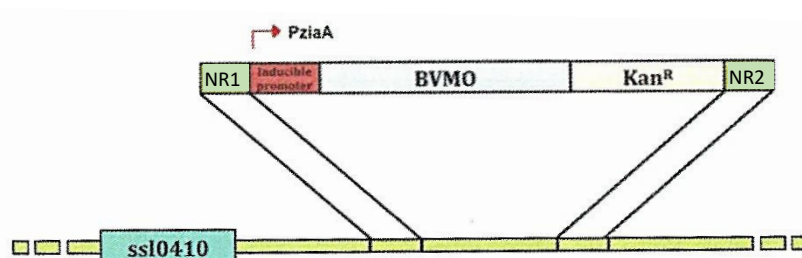
Stock solutions:

BG 1000X – total volume: 100 ml	
K_2HPO_4 (175 mM)	3,05 g
Na_2CO_3 (189 mM)	2 g
H_2O milliQ	Up to 100 ml

Trace mineral solution – total volume: 1 L	
H_3BO_4	2.86 g
$MnCl_2$ x 4 H_2O	1.81 g
$ZnSO_4$ x 7 H_2O	0.22 g
$NaMoO_4$ x 2 H_2O	0.39 g
$CuSO_4$ x 5 H_2O	0.08 g
$Co(NO_3)$ x 6 H_2O	0.05 g
H_2O milliQ	Up to 1L

BG FPC 100X – total volume: 1 L	
$NaNO_3$	149.58 g
$MgSO_4$ x 7 H_2O	7.49 g
$CaCl_2$ x 2 H_2O	3.6 g
Citric acid	0.92 g
0.25 M NaEDTA pH 8.0	1.12 ml
Trace mineral solution	100 ml
H_2O milliQ	Up to 1L

Ferric ammonium citrate 6 mg/ml	6 g / 1 L H_2O milliQ

0.25 NaEDTA pH 8.0	EDTA 46,5 g/ 500 ml H_2O milliQ. Adjust the pH to 8.0 with NaOH

TES-KOH 1M pH 8.2	TES 229,2 g/ 1 L H_2O milliQ. Adjust the pH to 8.2 with KOH

BG11 MEDIUM:

LIQUID BG11 MEDIUM – total volume:1L	
BG FCP 100X	10 ml
TES-KOH 1M pH 8.2	10 ml
BG 1000X	1 ml
Ferric ammonium citrate 6 mg/ml	1 ml
H_2O milliQ	Up to 1L

SOLID BG11 MEDIUM – total volume: 1L	
Liquid BG11 medium	1 L
Agar	15 g
Sodium Thiosulphate	3 g

For nitrogen-less BG11 medium, $NaNO_3$ was substituted with NaCl and $Co(NO_3)$ with $CoCl_2$

48

7.2 Methods

7.2.1 RNA extraction from *Synechocystis*

Total RNA was extracted from *Synechocystis* cells with NucleoSpin® RNA Plant Kit (Macherey-Nagel). Cells were pelleted by centrifuging 15 ml of culture (OD_{730} =2) at 6000g for 8 minutes at 4°C. The supernatant was discarded and then the given protocol was followed, starting from the lysis of the cells with Buffer RA1 (step 2).

7.2.2 RT-PCR (Polymerase Chain Reaction)

The total RNA extracted was retrotranscribed into cDNA (first strand) using SuperScript II® First-Strand Synthesis System (Invitrogen) with Random Primers (Promega), following the given protocol. The cDNA samples were subjected to semi-quantitative PCR for the amplification of *Cm*BVMO transcripts (primers SBVMO1f and SBVMO1r) and PetB transcripts (primers SpetB1f and SpetB1r). The composition of the reaction mix, together with the thermocycler settings, are given below.

dNTPs		0,5 µl
Buffer 5X		5 µl
$MgCl_2$		1,5 µl
DMSO		0,75 µl
Forward primer	SBVMO1f	1 µl
	SpetB1f	
Reverse primer	SBVMO1r	1 µl
	SpetB1r	
H_2O		10,05 µl
GoTaq		0,2 µl
Sample (cDNA)		5 µl
Total volume		25 µl

	Temperature	Time
1. Initial denaturation	95°C	2 min
2.Denaturation	95°C	1 min
3.Annealing	58°C	1 min
4.Extension	72°C	30 sec
5.Final extension	72°C	10 min
Steps 2,3,4 repeated 22 times		

7.2.3 Protein extraction from *Synechocystis*

Total protein content of *Synechocystis* cells was obtained using the following protocol:

- Centrifuge 10 ml of culture (OD730 =4) at 6000g for 8 minutes at 4°C.
- Discard supernatant and resuspend the pellet in 1.2 ml of Washing Buffer (50 mM Hepes-NaOH pH 7.5, 30 mM CaCl).
- Centrifuge the samples at 6000g for 8 minutes at 4°C and discard supernatant.

- Resuspend the pellet in 100 µl of Resuspension Buffer (50 mM Hepes-NaOH pH 7.5, 30 mM CaCl, 800 mM sorbitol, 1 mM ε-amino-n-caproic acid) and add the same volume of glass beads (150-212 µm, Sigma G-1145).
- Break the cells with Beadbeater at the maximum speed for 30 seconds
- Place the vials in ice for 2 minutes
- Repeat the last two passages for a total of 5 cycles
- Add 50 µl of Resuspension Buffer and repeat a cycle of Beadbeater for 5 seconds.
- Centrifuge at 1500g for 2 minutes at 4°C
- Transfer carefully the supernatant in a new vial, avoiding the beads
- Conserve at -20°C.

The concentration of total proteins was quantified using Bradford reagent, following the protocol for Microassay given by Bio-Rad.

7.2.4 SDS-PAGE

Protein electrophoresis was performed using a 10%-acrylamide gel with 6M urea, with the following composition:

Running gel		Stacking gel	
Urea	3.63 g	H_2O milliQ	1.62 ml
H_2O milliQ	2.09 ml	Tris 0,313 M, pH 6.8	1 ml
Tris 3M, pH 8.83	2.67 ml	Acrylamide 40%	0.375 ml
Acrylamide 40%	2.5 ml	TEMED	3.5 µl
TEMED	5.5 µl	APS 10%	35 µl
APS 10%	55 µl		

The gel is polymerised between two glass slides separated by two 1.5-mm-thick spacers, placed in the electrophoresis unit (Hoefer TM SE 260) and immersed in the Running Buffer (Tris 25 mM, glycine 192 mM, 0.1% w/v SDS). The samples are prepared with a Solubilisation Buffer (SB) composed of Tris 125 mM pH 6.8, DTT 100 mM, 20% glycerol, 9% SDS and Bromophenol Blue. After the loading of the samples, the electrophoretic run is performed at a current of 13 mA through the stacking gel, and then 25-30 mA through the running gel.

7.2.6 Western blot

A piece of PVDF membrane (polyvinylidene fluoride), having the same size as the acrylamide gel, is activated in methanol and washed in deionised water. The transfer blot is assembled placing in this precise order: a sponge, two sheet of blotting paper, PVDF membrane, acrylamide gel, other two sheet of blotting paper and another sponge. The system is placed in the western blotting apparatus and immersed in the Transfer Buffer ($NaHCO_3$ 10 mM, $NaCO_3$ 3 mM, 10% methanol). For the transfer, a current of 200 mA is applied over night at 4°C. The membrane is then washed in deionised water and prepared for the immunoblot. Before the

incubation with the primary antibody, the membrane is immersed in a solution of TBS (Tris-buffered saline; Tris 10 mM, NaCl 150 mM) and 10% milk powder, to reduce aspecific interactions. After 1 hour in agitation, the membrane is washed in TBS every 5 minutes for a total of 6 times and then incubated with the primary antibody (anti-BVMO) diluted 1:5000 in TTBS (Tween-TBS; Tris 10 mM, NaCl 150 mM, 0.05% Tween 20) and 5% milk powder. After 2 hours in agitation, the membrane is washed in TBS every 5 minutes for a total of 6 times and incubated with the secondary antibody (anti-rabbit) conjugated to HRP (horseradish peroxidase), diluted 1:20000 in TTBS. After 1 hour in agitation, the membrane is washed in TTBS every 5 minutes for a total of 6 times. The membrane is then immersed in a solution of 1:1 luminol:hydrogen peroxide for 5 minutes and in the darkroom is placed in a sealed system with a photographic plate. After an exposure time of approximatively 30 minutes, the plate is treated with the developing and fixing solutions.

7.2.7 Growth curves

- Starting from cells grown on agar plates, pre-inocula are set in 20 ml of BG11 liquid medium starting from an OD_{730} of 0,1 (5 mM glucose is added if the growth curve will be performed mixotrophically).
- After two days, the pre-inocula are pelleted at 4000g for 8 minutes at 25°C and resuspended in fresh BG11 medium, adjusting the OD_{730} at 0,1. Where needed, 5 mM glucose is added.
- The strains are put in agitation under continuous light illumination, at an intensity of 25 µmol s^{-1} m^{-2} at 30°C

7.2.8 Dry cell weight

- A membrane filter with a cut-off of 0,22 µm (Porafil®, Macherey-Nagel) is put in the heat dryer for 2 hours to be completely dried and its weight is registered
- The filter is placed on the top of a stainless-steel funnel on a Buchner flask, put under vacuum with a pump
- A sample of 10 ml of liquid culture is poured on top of the filter and the vacuum must be applied until all the liquid has passes inside the flask
- The filter with the cells is put in the heat dryer over night and then its weight is registered
- The difference between the first and the second weight gives the weight of the cells

7.2.9 Electronic Microscopy

The preparation and analysis of the samples have been carried out by the Optic and Electronic Microscopy Service of the Biology Department of Padua University. The samples were taken from standard mixotrophic cultures.

7.2.10 IMAC Chromatography

The affinity chromatography allows to purify proteins containing a 6x-histidine tag. This tag interacts with the nickel ions immobilized on a solid support (in our case, agarose spheres) binding firmly. The interaction is weakened with imidazole to allow the recovery of the his-tagged proteins.

The resin was incubated for 30 minutes with the soluble extract of *Synechocystis* cells (see par 7.2.3). After some washing steps, elution with Tris-imidazole 250mM was performed. Removal of imidazole was achieved by washing with Tris-HCl 50 mM through Vivaspin® columns (Sartorius).

7.2.11 Enzymatic activity assay

Reaction mixes were prepared in Tris-HCl 50 mM for the measure of NADPH absorbance at 340 nm, with a total volume of 100 µl for each reaction in a quartz cuvette. Where needed, the components were added with the following final concentrations: NADPH 0,2 mM, *Cm*BVMO 0,34 mg/ml, 3-nonanone 10 mM, hexadecanal 1,25 mM. After the addition of the last component needed, the absorbance was immediately registered, with a measure every 0,5 seconds, for 1 minute.

7.2.12 Native gel electrophoresis

Native gels were prepared with the following composition:

Running gel				Stacking gel
	4%	12%	20%	
Acrylamide 40%	0,54 ml	1,38 ml	2,30 ml	0,8 ml
H$_2$O milliQ (cold)	3 ml			4,52 ml
Gel Buffer 3X	1,8 ml	1,52 ml	1,52 ml	2,68 ml
TEMED	2,32 µl	1,52 µl	1,52 µl	6,4 µl
APS 10%	60 µl	40 µl	40 µl	64 µl
Glycerol 40%		1,85 ml	Glycerol 80%: 0,925 ml	

Gel Buffer: 50 mM BisTris-HCl pH 7, 645 mM ε-amino-n-caproic acid.

The acrylamide gradient was created using the Gradient Maker system (Elettrofor).

The samples were prepared diluting the protein extract (see par 7.2.3) in Tris-HCl 50 mM, to the proper concentration. 5 µl of BlueG was added to each sample while n-dodecylmaltoside was added to a final concentration of 1,5%.

After the loading of the samples, the electrophoretic run was performed at a current of 5 mA through the stacking gel, and then 2 mA through the running gel over night.

The running buffers were the Anode buffer (50 mM BisTris-HCl pH 7) and the Catode buffer (15 mM BisTris-HCl pH 7, 50 mM tricine, 0,02% BlueG).

For the colorimetric assay, the gel portions were incubated with a 5-ml solution of Tris-HCl 50 mM containing: 1 mg/ml NBT (Nitroblue tetrazolium), 0,2 mM NADPH, 10 mM 3-nonanone (only where needed). After 30 minutes of motionless incubation, the reaction was stopped with a solution containing 10% acetic acid.

7.2.13 Oxygen evolution measures

The oxygen electrode was prepared as indicated by the producer. Samples of liquid culture were diluted to reach an OD_{730} of 1. The electrode chamber was filled with 2 ml of the diluted samples and the oxygen level was monitored along time in the chamber without light. The slope of the curve was registered as the respiration rate. Then, light was turned on inside the chamber with an intensity of 3600 µmol s^{-1} m^{-2}. Again, the oxygen level was monitored along time. The slope of this curve was registered as the oxygen evolution rate due to the combination of photosynthesis and respiration. The difference between these two rates provides the net photosynthetic oxygen evolution.

7.2.14 Chlorophyll extraction

Samples from liquid cultures were centrifuged at 10000g for 5 minutes at 25°C and the supernatant was discarded. The pellet was smashed with a plastic pestle and resuspended in 1 ml of methanol. After a centrifugation at 10000g for 5 minutes at 25°C, the methanol extract was transferred to a quartz cuvette and, if too concentrated, diluted with methanol. The absorption spectra were collected and the absorbance of the 660-nm peak was used to normalise the oxygen evolution measures.

7.2.15 PHB quantification and visualization

Nitrogen starvation for PHB quantification was performed pelleting standard cultures and resuspending them in nitrogen-less BG11 medium, at an initial OD_{730} of 0,4. Na acetate was added at a final concentration of 10 mM. To 20 µL of cell culture, 6.6 µL Nile red solution (1 µg/ ml in ethanol) was added. The fluorescence emission at 590 nm was registered with the fluorescence spectrophotometer, with excitation at 544 nm.

Using a cell counter (Cellometer AutoX4, Nexcelon Bioscience), the relationship between OD_{730} and cell density was established to be the following: an OD_{730} of 1 corresponds to 10^8 cells/ml. By this proportion, the fluorescence was normalised on the number of cells.

PHB granules were visualized by staining with the fluorescent dye Nile red. To 20 µL of cell culture, 6.6 µL Nile red solution (1 µg/ ml in ethanol) was added. Of this mixture, 10 µL were dropped on a 2% agarose pad that was previously dried on a glass slides. The cells were analysed by fluorescence microscopy using a Leica microscope with a 100x/1.3 oil objective lens (Leica Microsystems).

7.2.16 GC-MS analysis

The GC-MS analysis was performed by Department of Chemistry of Padua University by kind permission and technical supervision of professor Andrea Sartorel.

7.2.17 Genomic DNA extraction from *Synechocystis*

Standard cultures, grown up to $OD_{730}=1$, were centrifuged at 6000g for 10 minutes at 25°C. Then, the following protocol was used:

- Resuspend the pellet in 125 µl of a saturated solution of NaI (184 g in 100 ml H_2O)
- Incubate at 37°C for 30 minutes in agitation and then centrifuge at 6000g for 10 minutes at 25°C
- Wash twice with deionised water
- Freeze the pellet at -80°C for 2 hours or over night
- Thaw and resuspend the pellet in 125 µl of Lysis Buffer (50 mM glucose, 50 mM Tris-HCl pH 8, 10 mM EDTA) at room temperature
- Add lysozyme to a final concentration of 15 mg/ml
- Mix and incubate at 37°C for 1 hour in agitation
- Add 250 µl of a solution containing NaOH 0,2% and SDS 1% (w/v)

- Incubate 10 minutes in ice
- Add 187,5 µl Na acetate 3M
- Incubate 30 minutes in ice
- Centrifuge at 12000g for 10 minutes at 4°C

The following steps must be performed under a fume hood:

- Transfer the supernatant, add the same volume of phenol:chloroform, vortex for 60 seconds, centrifuge at 14000g for 2 minutes at 4°C, recover the upper phase
- Repeat the previous step
- Add the same volume of chloroform 100%, vortex for 60 seconds, centrifuge at 14000g for 2 minutes at 4°C, recover the upper phase
- Add 1/10 (volume) of Na acetate 3M
- Add 2.5 volumes of ethanol 100%, previously stored at -20°C
- Vortex and incubate at -20°C for 3 hours or over night
- Centrifuge at 16000g for 30 minutes at 4°C and discard supernatant
- Wash twice with 1 ml ethanol 70% (v/v), previously stored at -20°C
- Centrifuge at 14000g for 10 minutes at 4°C
- Allow the pellet to dry under the fume hood
- Resuspend the pellet in sterile H_2O
- Add RNase (1:200) and incubate at 30 minutes at 37°C
- Store at -20°C

7.2.18 Knock-out constructs and *Synechocystis* cells transformation

A first PCR was performed on the wild type genome with Sll0209_for1 and Sll0209_rev2 to retrieve the whole sequence of sll0209 locus. By performing PCRs with Sll0209_KO1rev, KO2for, KO3rev and KO4for, the flanking regions FR1 and FR2 were amplified and linked together with a MCS (multiple cloning site). The construct was digested with XhoI and NotI and ligated with the plasmid pBSK-, previously digested with the same enzymes.

The MCS contained restriction sites for 4 endonucleases, and it was needed to insert the sequences for Kan^R and Cm^R, the resistance cassettes. Kan^R was excised from pUC4K with BamHI and ligated with the construct previously cut with BamHI. The same was done with CmR, excised from pUC4CAT with PstI. The final constructs were linearized by digesting them with BstXI, to rise the recombination efficiency.

Samples of liquid cultures of the strains were collected and brought to a concentration of 10^{10}cells/ml in BG11 medium. For every transformation required, 200 µl of these samples were incubated with 600 ng of the linearized construct for 5 hours at 30°C in agitation. Then the samples were poured onto a nylon filter on solid BG11 agar plates (with 5 mM glucose). The next day, the nylon filter was moved to the plates containing 10 µg/ml of antibiotic(s).

The selection of the transformants continued with the picking of single colonies, which were transferred once to plates containing 25 µg/ml of antibiotic(s) and six times in plates containing 50 µg/ml of antibiotic(s). All the plates contained 5 mM glucose.

7.2.19 PCR (Polymerase Chain Reaction)

To check the correct transformation of the mutants, two PCRs were performed. The reaction mix is the same for both, apart from the primers used. Composition of the reaction mixture for PCR and temperature settings are reported below.

dNTPs		1 µl
Buffer 5X		5 µl
MgCl$_2$		1,5 µl
Forward primer	Sll0209_for1	1 µl
	Sll0209_rev2	
Reverse primer	Kanam01_w	1 µl
	Clor1_rev	
H$_2$O		14,3 µl
GoTaq		0,2 µl
sample		1 µl
Total volume		25 µl

	Temperature	Time
1.Initial denaturation	95°C	30 sec
2.Denaturation	95°C	10 sec
3.Annealing	55°C	30 sec
4.Extension	72°C	30 sec
5.Final extension	72°C	10 min
Steps 2,3,4 repeated 30 times		

To check the homoplasmy for the mutants, a PCR was performed with Sll0209_for1 and Sll0209_rev2. Composition of the reaction mixture for PCR and temperature settings are reported below.

dNTPs	1 µl
Buffer 5X	5 µl
MgCl$_2$	1,5 µl
Forward primer: Sll0209_for1	1 µl
Reverse primer: Sll0209_rev2	1 µl
H$_2$O	14,3 µl
GoTaq	0,2 µl
sample	1 µl
Total volume	25 µl

	Temperature	Time
1.Initial denaturation	95°C	30 sec
2.Denaturation	95°C	10 sec
3.Annealing	60°C	30 sec
4.Exstension	72°C	90 sec
5.Final extension	72°C	10 min
Steps 2,3,4 repeated 30 times		

8. Bibliography

Ainas, M. *et al.* (2017) 'Hydrogen production with the cyanobacterium Spirulina platensis', *International Journal of Hydrogen Energy*. Pergamon, 42(8), pp. 4902–4907. doi: 10.1016/j.ijhydene.2016.12.056.

Angermayr, S. A. and Hellingwerf, K. J. (2013) 'On the use of metabolic control analysis in the optimization of cyanobacterial biosolar cell factories', *Journal of Physical Chemistry B*. American Chemical Society, 117(38), pp. 11169–11175. doi: 10.1021/jp4013152.

Aoki, S., Kondo, T. and Ishiura, M. (1995) 'Circadian expression of the dnaK gene in the cyanobacterium Synechocystis sp. strain PCC 6803', *Journal of Bacteriology*. American Society for Microbiology, 177(19), pp. 5606–5611. doi: 10.1128/jb.177.19.5606-5611.1995.

Balcerzak, L. *et al.* (2014) 'Biotransformations of monoterpenes by photoautotrophic micro-organisms', *Journal of Applied Microbiology*, pp. 1523–1536. doi: 10.1111/jam.12632.

Baldwin, C. V. F., Wohlgemuth, R. and Woodley, J. M. (2008) 'The first 200-L scale asymmetric Baeyer-Villiger oxidation using a whole-cell biocatalyst', *Organic Process Research and Development*, 12(4), pp. 660–665. doi: 10.1021/op800046t.

Bartsch, M. *et al.* (2015) 'Photosynthetic production of enantioselective biocatalysts.', *Microbial cell factories*. BioMed Central, 14(1), p. 53. doi: 10.1186/s12934-015-0233-5.

Beneventi, E. *et al.* (2013) 'Discovery of Baeyer-Villiger monooxygenases from photosynthetic eukaryotes', *Journal of Molecular Catalysis B: Enzymatic*, 98, pp. 145–154. doi: 10.1016/j.molcatb.2013.10.006.

Bentley, F. K., Zurbriggen, A. and Melis, A. (2014) 'Heterologous expression of the mevalonic acid pathway in cyanobacteria enhances endogenous carbon partitioning to isoprene', *Molecular Plant*, 7(1), pp. 71–86. doi: 10.1093/mp/sst134.

Bhati, R. and Mallick, N. (2015) 'Poly(3-hydroxybutyrate-co-3-hydroxyvalerate) copolymer production by the diazotrophic cyanobacterium Nostoc muscorum Agardh: Process optimization and polymer characterization', *Algal Research*. Elsevier, 7, pp. 78–85. doi: 10.1016/j.algal.2014.12.003.

Bisagni, S. *et al.* (2014) 'Exploring the substrate specificity and enantioselectivity of a baeyer-villiger monooxygenase from dietzia sp. D5: Oxidation of sulfides and aldehydes', *Topics in Catalysis*, 57(5), pp. 366–375. doi: 10.1007/s11244-013-0192-1.

Blasi, B. *et al.* (2012) 'Characterization of stress responses of heavy metal and metalloid inducible promoters in synechocystis PCC6803', *Journal of Microbiology and Biotechnology*, 22(2), pp. 166–169. doi: 10.4014/jmb.1106.06050.

Bode, H. B. *et al.* (2002) 'Big effects from small changes: Possible ways to explore nature's chemical diversity', *ChemBioChem*. WILEY-VCH Verlag GmbH, pp. 619–

627. doi: 10.1002/1439-7633(20020703)3:7<619::AID-CBIC619>3.0.CO;2-9.

Böhmer, S. *et al.* (2017) 'Enzymatic Oxyfunctionalization Driven by Photosynthetic Water-Splitting in the Cyanobacterium Synechocystis sp. PCC 6803', *Catalysts*. Multidisciplinary Digital Publishing Institute, 7(8), p. 240. doi: 10.3390/catal7080240.

Bordewick, S. *et al.* (2017) 'Baeyer-Villiger Monooxygenases from Yarrowia lipolytica Catalyze Preferentially Sulfoxidations Baeyer-Villiger Monooxygenases from Yarrowia lipolytica Catalyze Preferentially Sulfoxidations', *Enzyme and Microbial Technology*. Elsevier. doi: 10.1016/j.enzmictec.2017.09.008.

Bučko, M. *et al.* (2016) 'Baeyer-Villiger oxidations: biotechnological approach', *Applied Microbiology and Biotechnology*. Springer Berlin Heidelberg, pp. 6585–6599. doi: 10.1007/s00253-016-7670-x.

Busenlehner, L. S., Pennella, M. A. and Giedroc, D. P. (2003) 'The SmtB/ArsR family of metalloregulatory transcriptional repressors: Structural insights into prokaryotic metal resistance', *FEMS Microbiology Reviews*, pp. 131–143. doi: 10.1016/S0168-6445(03)00054-8.

Butinar, L. *et al.* (2015) 'Prevalence and specificity of Baeyer-Villiger monooxygenases in fungi', *Phytochemistry*. Pergamon, 117, pp. 144–153. doi: 10.1016/j.phytochem.2015.06.009.

Carpine, R. *et al.* (2017) 'Genetic engineering of Synechocystis sp. PCC6803 for poly-β-hydroxybutyrate overproduction', *Algal Research*. Elsevier, 25, pp. 117–127. doi: 10.1016/j.algal.2017.05.013.

de Carvalho, C. C. C. R. (2017) 'Whole cell biocatalysts: essential workers from Nature to the industry', *Microbial Biotechnology*, pp. 250–263. doi: 10.1111/1751-7915.12363.

Chaves, J. E. *et al.* (2017) 'Engineering Isoprene Synthase Expression and Activity in Cyanobacteria', *ACS Synthetic Biology*, p. acssynbio.7b00214. doi: 10.1021/acssynbio.7b00214.

Choi, S. Y. *et al.* (2016) 'Photosynthetic conversion of CO2 to farnesyl diphosphate-derived phytochemicals (amorpha-4,11-diene and squalene) by engineered cyanobacteria', *Biotechnology for Biofuels*, 9(1), p. 202. doi: 10.1186/s13068-016-0617-8.

Ciniglia, C. *et al.* (2004) 'Hidden biodiversity of the extremophilic Cyanidiales red algae', *Molecular Ecology*. Blackwell Science Ltd, 13(7), pp. 1827–1838. doi: 10.1111/j.1365-294X.2004.02180.x.

Collier, J. L. and Grossman, A. R. (1994) 'A small polypeptide triggers complete degradation of light-harvesting phycobiliproteins in nutrient-deprived cyanobacteria.', *The EMBO journal*. European Molecular Biology Organization, 13(5), pp. 1039–1047.

Davies, F. K. *et al.* (2014) 'Engineering Limonene and Bisabolene Production in Wild Type and a Glycogen-Deficient Mutant of Synechococcus sp. PCC 7002',

Frontiers in Bioengineering and Biotechnology. Frontiers, 2, p. 21. doi: 10.3389/fbioe.2014.00021.

Deng, M. De and Coleman, J. R. (1999) 'Ethanol synthesis by genetic engineering in cyanobacteria', *Applied and Environmental Microbiology*. American Society for Microbiology, 65(2), pp. 523–528.

Dismukes, G. C. *et al.* (2008) 'Aquatic phototrophs: efficient alternatives to land-based crops for biofuels', *Current Opinion in Biotechnology*. Elsevier Current Trends, pp. 235–240. doi: 10.1016/j.copbio.2008.05.007.

Donoghue, N. A., Norris, D. B. and Trudgill, P. W. (1976) 'The Purification and Properties of Cyclohexanone Oxygenase from Nocardia globerula CL1 and Acinetobacter NCIB 9871', *European Journal of Biochemistry*, 63(1), pp. 175–192. doi: 10.1111/j.1432-1033.1976.tb10220.x.

Ferroni, F. M. *et al.* (2017) 'Alkyl Formate Ester Synthesis by a Fungal Baeyer–Villiger Monooxygenase', *ChemBioChem*, 18(6), pp. 515–517. doi: 10.1002/cbic.201600684.

Field, L. M. *et al.* (2017) 'A comparison of protein extraction methods optimizing high protein yields from marine algae and cyanobacteria', *Journal of Applied Phycology*, 29(3), pp. 1271–1278. doi: 10.1007/s10811-016-1027-9.

Flores, F. G. (2008) *The cyanobacteria: molecular biology, genomics, and evolution*. Horizon Scientific Press.

Formighieri, C. and Melis, A. (2016) 'Sustainable heterologous production of terpene hydrocarbons in cyanobacteria', *Photosynthesis Research*, 130(1–3), pp. 123–135. doi: 10.1007/s11120-016-0233-2.

Fraaije, M. W. *et al.* (2002) 'Identification of a Baeyer-Villiger monooxygenase sequence motif', *FEBS Letters*. No longer published by Elsevier, 518(1–3), pp. 43–47. doi: 10.1016/S0014-5793(02)02623-6.

Fürst, M. J. L. J. *et al.* (2017) 'Polycyclic ketone monooxygenase from the thermophilic fungus Thermothelomyces thermophila: A structurally distinct biocatalyst for bulky substrates', *Journal of the American Chemical Society*. American Chemical Society, 139(2), pp. 627–630. doi: 10.1021/jacs.6b12246.

Geitner, K. *et al.* (2010) 'Scale-up of Baeyer-Villiger monooxygenase-catalyzed synthesis of enantiopure compounds', *Applied Microbiology and Biotechnology*. Springer-Verlag, 88(5), pp. 1087–1093. doi: 10.1007/s00253-010-2724-y.

Genty, B., Briantais, J. M. and Baker, N. R. (1989) 'The relatioship between the quantum yield of photosynthetic electron transport and quenching of chlorophyll fluorescence', *Biochimica et Biophysica Acta*, 990, pp. 87–92.

Golden, S. S., Brusslan, J. and Haselkorn, R. (1987) 'Genetic Engineering of the Cyanobacterial Chromosome', *Methods in Enzymology*. Academic Press, 153(C), pp. 215–231. doi: 10.1016/0076-6879(87)53055-5.

Górak, M. and Żymańczyk-Duda, E. (2015) 'Application of cyanobacteria for

chiral phosphonate synthesis', *Green Chem.* The Royal Society of Chemistry, 17(9), pp. 4570–4578. doi: 10.1039/C5GC01195G.

Griese, M., Lange, C. and Soppa, J. (2011) 'Ploidy in cyanobacteria', *FEMS Microbiology Letters*, 323(2), pp. 124–131. doi: 10.1111/j.1574-6968.2011.02368.x.

Hauf, W. *et al.* (2013) 'Metabolic changes in Synechocystis PCC6803 upon nitrogen-starvation: Excess NADPH sustains polyhydroxybutyrate accumulation', *Metabolites*, 3(1), pp. 101–118. doi: 10.3390/metabo3010101.

Havel, J. and Weuster-Botz, D. (2006) 'Comparative study of cyanobacteria as biocatalysts for the asymmetric synthesis of chiral building blocks', *Engineering in Life Sciences*. WILEY-VCH Verlag, 6(2), pp. 175–179. doi: 10.1002/elsc.200620909.

Ikeuchi, M. and Tabata, S. (2001) 'Synechocystis sp. PCC 6803 - a useful tool in the study of the genetics of cyanobacteria.', *Photosynthesis research*, 70(1), pp. 73–83. doi: 10.1023/A:1013887908680.

Kamerbeek, N. M. *et al.* (2001) '4-Hydroxyacetophenone monooxygenase from Pseudomonas fluorescens ACB', *European Journal of Biochemistry*, 268(9), pp. 2547–2557. doi: 10.1046/j.1432-1327.2001.02137.x.

Kamerbeek, N. M. *et al.* (2003) 'Substrate specificity and enantioselectivity of 4-hydroxyacetophenone monooxygenase', *Applied and Environmental Microbiology*, 69(1), pp. 419–426. doi: 10.1128/AEM.69.1.419-426.2003.

Kaneko, T. *et al.* (1996) 'Sequence Analysis of the Genome of the Unicellular Cyanobacterium Synechocystis sp. Strain PCC6803. II. Sequence Determination of the Entire Genome and Assignment of Potential Protein-coding Regions', *DNA Research*, 3(3), pp. 109–136. doi: 10.1093/dnares/3.3.109.

Koeller, K. M. and Wong, C. H. (2001) 'Enzymes for chemical synthesis.', *Nature*. Nature Publishing Group, 409(6817), pp. 232–240. doi: 10.1038/35051706.

Kosourov, S., Murukesan, G. and Allahverdiyeva, Y. (2017) 'Evaluation of light energy to H2 energy conversion efficiencies in immobilized cyanobacteria and green algae under autotrophic conditions', *Algal Research*. Elsevier, p. submitted. doi: 10.1016/j.algal.2017.09.027.

Kramer, D. M. and Evans, J. R. (2011) 'The Importance of Energy Balance in Improving Photosynthetic Productivity', *PLANT PHYSIOLOGY*. American Society of Plant Biologists, 155(1), pp. 70–78. doi: 10.1104/pp.110.166652.

Kucho, K. *et al.* (2005) 'Improvement of the bioluminescence reporter system for real-time monitoring of circadian rhythms in the cyanobacterium Synechocystis sp. strain PCC 6803', *Genes & Genetic Systems*. The Genetics Society of Japan, 80(1), pp. 19–23. doi: 10.1266/ggs.80.19.

Kyte, B. G. *et al.* (2004) 'Assessing the Substrate Selectivities and Enantioselectivities of Eight Novel Baeyer-Villiger Monooxygenases toward Alkyl-Substituted Cyclohexanones', *Journal of Organic Chemistry*, 69(1), pp. 12–17. doi: 10.1021/jo030253l.

Leipold, F., Wardenga, R. and Bornscheuer, U. T. (2012) 'Cloning, expression and characterization of a eukaryotic cycloalkanone monooxygenase from Cylindrocarpon radicicola ATCC 11011', *Applied Microbiology and Biotechnology*. Springer-Verlag, 94(3), pp. 705–717. doi: 10.1007/s00253-011-3670-z.

Li, X., Shen, C. R. and Liao, J. C. (2014) 'Isobutanol production as an alternative metabolic sink to rescue the growth deficiency of the glycogen mutant of Synechococcus elongatus PCC 7942', *Photosynthesis Research*. Springer Netherlands, 120(3), pp. 301–310. doi: 10.1007/s11120-014-9987-6.

Lin, B. and Tao, Y. (2017) 'Whole-cell biocatalysts by design', *Microbial Cell Factories*, 16(1), p. 106. doi: 10.1186/s12934-017-0724-7.

Liu, X., Sheng, J. and Curtiss III, R. (2011) 'Fatty acid production in genetically modified cyanobacteria', *Proceedings of the National Academy of Sciences*, 108(17), pp. 6899–6904. doi: 10.1073/pnas.1103014108.

Luan, G. *et al.* (2015) 'Combinatory strategy for characterizing and understanding the ethanol synthesis pathway in cyanobacteria cell factories', *Biotechnology for Biofuels*. BioMed Central, 8(1), p. 184. doi: 10.1186/s13068-015-0367-z.

Malito, E. *et al.* (2004) 'Crystal structure of a Baeyer-Villiger monooxygenase.', *Proceedings of the National Academy of Sciences of the United States of America*, 101(36), pp. 13157–62. doi: 10.1073/pnas.0404538101.

Manivannan, P., Muralitharan, G. and Balaji, N. P. (2017) 'Prediction aided in vitro analysis of octa-decanoic acid from Cyanobacterium Lyngbya sp. as a pro-apoptotic factor in eliciting anti-inflammatory properties'.

Marcus, Y. *et al.* (2011) 'Rubisco mutagenesis provides new insight into limitations on photosynthesis and growth in Synechocystis PCC6803', *Journal of Experimental Botany*. Oxford University Press, 62(12), pp. 4173–4182. doi: 10.1093/jxb/err116.

Mascotti, M. *et al.* (2013) 'Cloning, overexpression and biocatalytic exploration of a novel Baeyer-Villiger monooxygenase from Aspergillus fumigatus Af293', *AMB Express*. Springer Berlin Heidelberg, 3(1), p. 33. doi: 10.1186/2191-0855-3-33.

Moonen, M. J. H. *et al.* (2005) 'Enzymatic Baeyer-Villiger oxidation of benzaldehydes', *Advanced Synthesis and Catalysis*, 347(7–8), pp. 1027–1034. doi: 10.1002/adsc.200404307.

Morii, S. *et al.* (1999) 'Steroid Monooxygenase of Rhodococcus rhodochrous: Sequencing of the Grenomic DNA, and Hyperexpression, Purification, and Characterization of the Recombinant Enzyme', *Journal of Biochemistry*. Oxford University Press, 126(3), pp. 624–631. doi: 10.1093/oxfordjournals.jbchem.a022494.

Nakamura, K. *et al.* (2000) 'Cyanobacterium-catalyzed asymmetric reduction of ketones', *Tetrahedron Letters*. Pergamon, 41(35), pp. 6799–6802. doi: 10.1016/S0040-4039(00)01132-1.

Ochoa de Alda, J. A. G. *et al.* (2014) 'The plastid ancestor originated among one of the major cyanobacterial lineages', *Nature Communications*. Nature Publishing

Group, 5, p. 4937. doi: 10.1038/ncomms5937.

Pade, N. *et al.* (2016) 'Insights into isoprene production using the cyanobacterium Synechocystis sp. PCC 6803', *Biotechnology for Biofuels*, 9(1), p. 89. doi: 10.1186/s13068-016-0503-4.

Panda, B. *et al.* (2006) 'Optimization of cultural and nutritional conditions for accumulation of poly-β-hydroxybutyrate in Synechocystis sp. PCC 6803', *Bioresource Technology*. Elsevier, 97(11), pp. 1296–1301. doi: 10.1016/j.biortech.2005.05.013.

Panda, B. and Mallick, N. (2007) 'Enhanced poly-β-hydroxybutyrate accumulation in a unicellular cyanobacterium, Synechocystis sp. PCC 6803', *Letters in Applied Microbiology*, 44(2), pp. 194–198. doi: 10.1111/j.1472-765X.2006.02048.x.

Park, J. and Choi, Y. (2017) 'Cofactor engineering in cyanobacteria to overcome imbalance between NADPH and NADH: A mini review', *Frontiers of Chemical Science and Engineering*, 11(1), pp. 66–71. doi: 10.1007/s11705-016-1591-1.

Rahman, D. Y. *et al.* (2017) 'Thermostable phycocyanin from the red microalga Cyanidioschyzon merolae, a new natural blue food colorant', *Journal of Applied Phycology*. Springer Netherlands, 29(3), pp. 1233–1239. doi: 10.1007/s10811-016-1007-0.

Rippka, R. *et al.* (1979) 'Generic Assignments, Strain Histories and Properties of Pure Cultures of Cyanobacteria', *Microbiology*. Microbiology Society, 111(1), pp. 1–61. doi: 10.1099/00221287-111-1-1.

Romero, E. *et al.* (2016) 'Characterization and Crystal Structure of a Robust Cyclohexanone Monooxygenase', *Angewandte Chemie - International Edition*, 55(51), pp. 15852–15855. doi: 10.1002/anie.201608951.

Ruffing, A. M. (2014) 'Improved Free Fatty Acid Production in Cyanobacteria with Synechococcus sp. PCC 7002 as Host', *Frontiers in Bioengineering and Biotechnology*, 2. doi: 10.3389/fbioe.2014.00017.

Samantaray, S. and Mallick, N. (2012) 'Production and characterization of poly-β-hydroxybutyrate (PHB) polymer from Aulosira fertilissima', *Journal of Applied Phycology*. Springer Netherlands, 24(4), pp. 803–814. doi: 10.1007/s10811-011-9699-7.

Sheldon, R. A. and Woodley, J. M. (2017) 'Role of Biocatalysis in Sustainable Chemistry', *Chemical Reviews*. American Chemical Society, p. acs.chemrev.7b00203. doi: 10.1021/acs.chemrev.7b00203.

Simmons, T. L. *et al.* (2005) 'Marine natural products as anticancer drugs', *Molecular Cancer Therapeutics*. American Association for Cancer Research, 4(February), pp. 333–342.

Singh, A. K. *et al.* (2008) 'Integration of Carbon and Nitrogen Metabolism with Energy Production Is Crucial to Light Acclimation in the Cyanobacterium Synechocystis', *PLANT PHYSIOLOGY*, 148(1), pp. 467–478. doi:

10.1104/pp.108.123489.

Singh, A. K. *et al.* (2017) *Progress and challenges in producing polyhydroxyalkanoate biopolymers from cyanobacteria*, *Journal of Applied Phycology*. doi: 10.1007/s10811-016-1006-1.

Singh, R. S. *et al.* (2017) 'Cyanobacterial lectins characteristics and their role as antiviral agents', *International Journal of Biological Macromolecules*. Elsevier, pp. 475–496. doi: 10.1016/j.ijbiomac.2017.04.041.

Stephen, A. J. *et al.* (2017) 'Advances and bottlenecks in microbial hydrogen production', *Microbial Biotechnology*, 10(5), pp. 1120–1127. doi: 10.1111/1751-7915.12790.

Swain, S. S., Paidesetty, S. K. and Padhy, R. N. (2017) 'Antibacterial, antifungal and antimycobacterial compounds from cyanobacteria', *Biomedicine and Pharmacotherapy*. Elsevier Masson, pp. 760–776. doi: 10.1016/j.biopha.2017.04.030.

Tang, X. S. and Diner, B. A. (1994) 'Biochemical and spectroscopic characterization of a new oxygen-evolving photosystem II core complex from the cyanobacterium Synechocystis PCC 6803.', *Biochemistry*, 33(15), pp. 4594–4603.

Torres Pazmiño, D. E. *et al.* (2008) 'Kinetic mechanism of phenylacetone monooxygenase from Thermobifida fusca', *Biochemistry*. American Chemical Society, 47(13), pp. 4082–4093. doi: 10.1021/bi702296k.

Tsujimoto, R., Kamiya, N. and Fujita, Y. (2016) 'Identification of a cis-acting element in nitrogen fixation genes recognized by CnfR in the nonheterocystous nitrogen-fixing cyanobacterium Leptolyngbya boryana', *Molecular Microbiology*, 101(3), pp. 411–424. doi: 10.1111/mmi.13402.

Wang, C., Kim, J.-H. and Kim, S.-W. (2014) 'Synthetic Biology and Metabolic Engineering for Marine Carotenoids: New Opportunities and Future Prospects', *Marine Drugs*, 12(9), pp. 4810–4832. doi: 10.3390/md12094810.

Wang, M. *et al.* (2017) 'Cofactor engineering for more efficient production of chemicals and biofuels', *Biotechnology Advances*. Elsevier. doi: 10.1016/j.biotechadv.2017.09.008.

Wang, X. *et al.* (2017) 'Cofactor NAD(P)H Regeneration Inspired by Heterogeneous Pathways', *Chem*. Cell Press, pp. 621–654. doi: 10.1016/j.chempr.2017.04.009.

Wang, Y. *et al.* (2016) 'Biosynthesis of platform chemical 3-hydroxypropionic acid (3-HP) directly from CO_2 in cyanobacterium Synechocystis sp. PCC 6803', *Metabolic Engineering*. Academic Press, 34, pp. 60–70. doi: 10.1016/j.ymben.2015.10.008.

Willetts, A. (1997) 'Structural studies and synthetic applications of Baeyer-Villiger monooxygenases', *Trends in Biotechnology*. Elsevier Current Trends, pp. 55–62. doi: 10.1016/S0167-7799(97)84204-7.

Work, V. H. *et al.* (2015) 'Lauric Acid Production in a Glycogen-Less Strain of

Synechococcus sp. PCC 7002', *Frontiers in Bioengineering and Biotechnology*, 3. doi: 10.3389/fbioe.2015.00048.

Yao, L. *et al.* (2014) 'Improved production of fatty alcohols in cyanobacteria by metabolic engineering', *Biotechnology for Biofuels*, 7(1), p. 94. doi: 10.1186/1754-6834-7-94.

Yoshino, T. *et al.* (2014) 'Alkane production by the marine cyanobacterium Synechococcus sp. NKBG15041c possessing the α-olefin biosynthesis pathway', *Applied Microbiology and Biotechnology*. Springer Berlin Heidelberg, 99(3), pp. 1521–1529. doi: 10.1007/s00253-014-6286-2.

Zhou, J. *et al.* (2015) 'Discovery of a super-strong promoter enables efficient production of heterologous proteins in cyanobacteria', *Scientific Reports*. Nature Publishing Group, 4(1), p. 4500. doi: 10.1038/srep04500.

Zhou, J. *et al.* (2016) 'Introducing extra NADPH consumption ability significantly increases the photosynthetic efficiency and biomass production of cyanobacteria', *Metabolic Engineering*. Academic Press, 38, pp. 217–227. doi: 10.1016/j.ymben.2016.08.002.

Acknowledgements – Ringrazimenti